Solution Structure of Human Type-α Transforming Growth Factor Determined by Heteronuclear NMR Spectroscopy and Refined by Energy Minimization with Restraints†,‡

Franklin J. Moy,§,∥ Yu-Chin Li,∥ Peter Rauenbuehler,⊥ Marjorie E. Winkler,⊥ Harold A. Scheraga,*,§ and Gaetano T. Montelione*,∥

Baker Laboratory of Chemistry, Cornell University, Ithaca, New York 14853-1301, Center for Advanced Biotechnology and Medicine and The Graduate Program in Chemistry, Rutgers University, Piscataway, New Jersey 08854-5638, and Department of Recovery Process Research and Development and Quality Control, Genentech, Inc., 460 Point San Bruno Boulevard, South San Francisco, California 94080

Received October 14, 1992; Revised Manuscript Received February 18, 1993

ABSTRACT: Human type-α transforming growth factor (hTGFα) is a small mitogenic protein containing 50 amino acids and 3 disulfide bonds. Homo- and heteronuclear NMR spectra were used to determine nearly complete sequence-specific ^1H and ^{15}N resonance assignments for hTGFα under three conditions: pH 6.5 and a temperature of 10 °C, pH 6.5 and a temperature of 30 °C, and pH 3.5 and a temperature of 30 °C. The ^{15}N-enriched samples of hTGFα allowed determination of many $^3J(H^N–H^\alpha)$ vicinal coupling constants. Solution structures of human type-α transforming growth factor (hTGFα) at pH 6.5 and a temperature of 10 °C were determined from NMR data using molecular structure generation calculations and restrained energy minimization. These structures are based on 425 conformational constraints, including 357 NOE-derived upper-bound distance constraints, constraints on the ranges of 26 dihedral angles based on measurements of vicinal coupling constants, 42 upper- and lower-bound constraints associated with 6 hydrogen bonds and 3 disulfide bonds, and several stereospecific ^1H resonance assignments. The overall structure is similar to that described recently for hTGFα by other groups [Kline et al. (1990) *Biochemistry 29*, 7805–7813; Harvey et al. (1991) *Eur. J. Biochem. 198*, 555–562], but there are differences in some structural details. The resonance frequencies, vicinal coupling constants, and NOEs form the basis for comparisons of the solution structure of hTGFα at neutral and acidic pH. At pH 3.5 the protein structure is partially disordered, with most of the hydrogen-bonded backbone structure still intact. The hTGFα structure is also compared with that of murine epidermal growth factor. Coordinates for the set of hTGFα structures described in this paper have been deposited in the Protein Data Bank.

Type-α transforming growth factor (TGFα)[1] is a small mitogenic protein containing 50 amino acids and 3 disulfide bonds. It has about 30% sequence identity with epidermal growth factor (EGF) (Simpson et al., 1985; Campbell et al., 1989). Originally discovered in cultured media of murine sarcoma virus-transformed cells (De Larco & Todaro, 1978), TGFα acts synergistically with other growth factors, including type-β TGF (TGFβ), to induce phenotypic transformation in certain cell lines (Roberts et al., 1981; Anzano et al., 1983). TGFα and other EGF-like proteins appear to play an important role in the molecular basis of wound healing (Burgess, 1989) and oncogensis (Sporn & Todaro, 1980; Sporn & Roberts, 1985; Heldin & Westermark, 1990). Although no crystal structures are yet available for any of the EGF-like proteins, low-resolution solution structures derived from NMR measurements are available for human TGFα (hTGFα) (Brown et al., 1989; Campbell et al., 1989; Kohda et al., 1989; Montelione et al., 1989; Tappin et al., 1989; Kline et al., 1990; Harvey et al., 1991), human EGF (hEGF) (Carver et al., 1986; Cooke et al., 1987), murine EGF (mEGF) (Montelione et al., 1986, 1987, 1992; Kohda & Inagaki, 1988, 1992a; Kohda et al., 1988), micelle-bound mEGF (Kohda & Inagaki, 1992b), rat EGF (Mayo et al., 1989), the EGF-like domain from bovine coagulation factor X (Selander et al., 1990), and the EGF-like module of human factor IX (Huang et al., 1991; Baron et al., 1992). For all of these molecules, the backbone structures are very similar to that first described for murine

† This work was supported by the National Institutes of Health (Grants GM-24893 and GM-47014), the Cornell Biotechnology Program, the National Science Foundation (Grant DIR-9019313), and the Searle Scholars Program/Chicago Community Trust. Support was also received from the National Foundation for Cancer Research. This work is part of the Ph.D. Thesis in Chemistry of F.J.M. at Cornell University.

‡ Atomic coordinates have been deposited in the Brookhaven Protein Data Bank.

* To whom correspondence should be addressed.

§ Cornell University.

∥ Rutgers University.

⊥ Genentech, Inc.

[1] Abbreviations: CD, circular dichroism; ECEPP, empirical conformational energy program for peptides; EGF, epidermal growth factor; mEGF, murine EGF; hEGF, human EGF; OD, optical density; TGFα, type-α transforming growth factor; hTGFα, human TGFα; 1D, one dimensional; 2D, two dimensional; 3D, three dimensional; COSY, 2D correlated spectroscopy; COSY-30, COSY experiment using a final pulse with a 30° flip angle; 2QF-COSY, 2D two-quantum filtered COSY; relayed-COSY, relayed coherence transfer spectroscopy; DISMAN, program used to calculate molecular structures from internuclear distance constraints; FID, free induction decay; HMQC, 2D ^{15}N–^1H heteronuclear multiple-quantum coherence spectroscopy; HSQC, 2D ^{15}N–^1H heteronuclear single-quantum coherence spectroscopy; NOE, nuclear Overhauser effect; NOESY, 2D NOE spectroscopy; TOCSY, 2D total correlation spectroscopy; HSQC–TOCSY, 2D NMR experiment combining HSQC and TOCSY; HSQC–NOESY, 2D NMR experiment combining HSQC and NOESY; 3D NOESY–HSQC, 3D NMR experiment combining NOESY and HSQC; HSQC-J, modified HSQC experiment with incremented delays; τ, $^3J(H^N–H^\alpha)$ evolution time in HSQC-J; τ_{inv}, value of τ in an HSQC-J experiment at which the $^1J(^{15}N–H^N)$ peak changes sign; τ_m, mixing time in NOESY; TPPI, time-proportional phase incrementation; GARP, multipulse heteronuclear decoupling scheme; MLEV, multipulse spin-locking scheme; REDAC, redundant dihedral angle constraints.

0006-2960/93/0432-7334$04.00/0

EGF (Montelione et al., 1986), with a three-stranded antiparallel β-sheet in the N-terminal two-thirds of the sequence and a small "double hairpin" structure in the C-terminal third of the sequence.

While the conformation of mEGF is relatively insensitive to pH in the range from 2 to 9 (Kohda et al., 1991), in hTGFα there is a pH-induced conformational transition associated with the titration of several histidine residues (Tappin et al., 1989). One difference between the hTGFα structure at neutral and acidic pH is that the N-terminal strand of the triple-stranded β-sheet structure present at neutral pH (Tappin et al., 1989; Kline et al., 1990; Harvey et al., 1991) is disrupted at acidic pH (Brown et al., 1989; Montelione et al., 1989; Tappin et al., 1989). In addition, studies of the temperature dependence of one-dimensional (1D) NMR spectra (Tappin et al., 1989) indicate that the aromatic resonances of Tyr-38 are more susceptible to temperature-induced line broadening and frequency shifting at acidic pH than at neutral pH and that many amide resonances are significantly broader at pH 3.5 than at pH 6.5. These observations suggest a pH-dependent equilibrium between folded and partially unfolded forms of hTGFα at pH 3.5 (Tappin et al., 1989).

In 1989, four groups simultaneously described the first low-resolution solution structures of hTGFα (Brown et al., 1989; Kohda et al., 1989; Montelione et al., 1989; Tappin et al., 1989). These structures were based on mechanical models that were constructed to fit the experimental NMR data. Recently, more detailed atomic models based on distance geometry calculations have also been described for recombinant [des-Val-1–Val-2]hTGFα (Kline et al., 1990) and for intact hTGFα (Harvey et al., 1991). In both of these structure determinations, the atomic coordinates were generated by using distance geometry calculations followed by restrained molecular dynamics.

In considering the accuracy and precision of a molecular structure determination by crystallography or NMR, it is invaluable to have access to molecular coordinates generated for the same molecule by different laboratories. It is especially important to develop a data base of such parallel structure determinations by NMR spectroscopy in order to understand better the biases of different refinement procedures and to identify errors in interpretation of NMR data.

In this paper, we describe the structure determination of hTGFα at pH 6.5 and a temperature of 10 °C. The refined coordinates provide an alternative view of the detailed atomic structure of hTGFα than that available from the literature since our set of input constraints and strategy for generating these structures are significantly different from those used by other groups (Kline et al., 1990; Harvey et al., 1991). Proton-detected heteronuclear NMR measurements were also used to characterize the locations and amplitudes of the pH-induced structural changes in greater detail. These heteronuclear NMR data, together with homonuclear Overhauser effect spectroscopy (NOESY) data, provide a picture of the structural changes that occur in this molecule as the solution is shifted from neutral to acidic pH.

MATERIALS AND METHODS

Production of Recombinant hTGFα. Recombinant hTGFα was expressed as a *trp*LE fusion protein in *Escherichia coli* containing the pTE5 plasmid (Derynck et al., 1984). The initial purification, refolding, and cleavage of the fusion protein were carried out as described previously (Winkler et al., 1986), except that Sephacryl S-300 (Pharmacia) was substituted for Sephadex G-75.

^{15}N-Enrichment of hTGFα. *E. coli* containing the plasmid pTE5 were grown in synthetic media containing Trp-8 salts [25 mM monobasic sodium phosphate, 34 mM dibasic potassium phosphate, 3 mM sodium citrate, 5 g/L 100% ^{15}N-enriched ammonium sulfate (MSD Isotopes), 15.6 g/L glucose, 12.5 mM magnesium sulfate, 0.005% tryptophan, 0.00013% thiamin, 2.5 mg/L tetracycline, and trace elements]. Three additional increments of 10 g/L glucose each were added during the fermentation. In this plasmid, hTGFα expression is controlled by the *trp* promoter and was induced by the addition of 50 mg/L indoleacrylic acid when the optical density (OD) at 550 nm of the fermentation reached 14 units. Cells were harvested 8 h after induction, and the protein was then purified as described above. The yield of ^{15}N-enriched hTGFα based on immunochemical analysis was about 13 mg/L.

Final Purification. These preparations of hTGFα and ^{15}N-enriched hTGFα were found to be >95% homogeneous by C18 (Waters Chromatography) reversed-phase analytical HPLC. Further purification was carried out by using a preparative Mono S column (Pharmacia) with a gradient of NaCl in 50 mM sodium acetate at pH 5.2. In the final step, the protein was desalted by C18 reversed-phase chromatography. Analytical reversed-phase and cation-exchange chromatography indicated that these samples used for NMR studies are >98% homogeneous.

Circular Dichroism (CD) Spectroscopy. Far-ultraviolet CD spectra were obtained using an Aviv Model 62-DS spectropolarimeter. Samples were prepared at approximately 0.2 mM concentration in water at pH 3.5 (unbuffered) or 6.5 (buffered with 20 mM Na_2HPO_4). The CD-detected thermal transition curves obtained under these conditions were found to be fully reversible.

NMR Spectroscopy. Samples for NMR spectroscopy were prepared in aqueous solutions of 2–4 mM protein concentration at pH 3.5 ± 0.1 or pH 6.5 ± 0.1 containing 1 mM NaN_3. For ^2H_2O solutions, the pH meter reading is reported without correction for isotope effects. Protein samples in H_2O were prepared by dissolving the protein directly in 90% ^1H_2O/10% ^2H_2O (MSD Isotopes). Samples were prepared for measurements in ^2H_2O solutions by first exchanging all labile protons for deuterons at room temperature at pH 3.5 or 6.5, followed by two cycles of lyophilization in 100% ^2H_2O, and then dissolving the protein in 100% ^2H_2O. The same ^{15}N-TGFα sample in 90% ^1H_2O/10% ^2H_2O containing 1 mM NaN_3 was used for the pH 3.5 and 6.5 studies. We observed no evidence for protein aggregation in these samples.

Two-dimensional (2D) two-quantum filtered correlation spectroscopy (2QF-COSY) (Piantini et al., 1982), NOESY (Jeener et al., 1979; Kumar et al., 1980), total correlation spectroscopy (TOCSY) (Braunschweiler & Ernst, 1983; Davis & Bax, 1985), relayed coherence transfer spectroscopy (relayed-COSY) (Eich et al., 1982; Wagner, 1982), and ^{15}N heteronuclear single-quantum coherence spectroscopy (HSQC) (Bodenhausen & Ruben, 1980) NMR spectra were recorded on a Varian Unity 500 spectrometer. The pulse sequences used to obtain 2D HSQC–TOCSY, 2D HSQC–NOESY, and 3D NOESY–HSQC NMR spectra are presented in Figure S1 in the supplementary material. The HSQC versions of these ^{15}N-edited experiments exhibit higher signal-to-noise ratios than corresponding heteronuclear multiple-quantum coherence spectroscopy (HMQC) versions which have been described elsewhere (Fesik & Zuiderweg, 1988; Kay et al., 1989; Marion et al., 1989). To select multiplet components for $^3J(H^\alpha–H^\beta)$ coupling constant measurements, a modified

2D correlated spectroscopy (COSY-30) spectrum (Müller, 1987; Montelione et al., 1992) was recorded using 1024 data points in ω_1 and 8192 data points in ω_2. ^{1}H chemical shifts are reported in parts per million (ppm) relative to the methyl resonance of 2,2-dimethyl-2-silapentane-5-sulfonate (DSS), assigned as 0.0 ppm. ^{15}N chemical shifts are reported in parts per million (ppm) relative to external $^{15}NH_4Cl$, assigned as 24.9 ppm.

Measurements of $^3J(H^N–H^\alpha)$ Coupling Constants. Vicinal $^3J(H^N–H^\alpha)$ coupling constants were estimated using a modified version of the refocused HSQC experiment (Neri et al., 1990; Billeter et al., 1992). We call this experiment HSQC-J. In HSQC-J, the ^{15}N–^{1}H correlation peaks are modulated by $^3J(H^N–H^\alpha)$ coupling during the time period τ (Neri et al., 1990). The signs of the ^{15}N–^{1}H cross peaks invert approximately at $\tau_{inv} = 1/[2\,^3J(H^N–H^\alpha)]$. Accordingly, upper and lower bounds for the individual coupling constants $^3J(H^N–H^\alpha)$ are determined by the longest τ value for which the ^{15}N–^{1}H cross peaks retain the same sign as that observed at τ = 50 ms and the shortest τ value for which the signs are inverted, respectively. For each condition of pH and temperature, an array of 2D spectra were obtained with values τ = 50, 56, 63, 71, 83, 100, 125, and 167 ms corresponding to sign inversions for $^3J(H^N–H^\alpha)$ coupling constants of 10, 9, 8, 7, 6, 5, 4, and 3 Hz, respectively. In cases when the ^{15}N–^{1}H correlation peak disappears and never reappears at longer τ values because of T_2 relaxation processes, the lower-bound $^3J(H^N–H^\alpha)$ coupling constant value was conservatively set to 0 Hz. For each experiment 160 free induction decays of 64 scans each were collected.

Stereospecific Resonance Assignments. The stereospecific assignments of β-methylene protons and valine isopropyl methyl groups and the individual assignments of side-chain amide protons were determined by methods described previously (Montelione et al., 1992). The $H^N–H^\beta$, $H^\alpha–H^\beta$, $H^N–C^\gamma H_3$, $H^\alpha–C^\gamma H_3$, $H^\beta–H^\delta$ and H^γ-H^ϵ NOEs were estimated from NOESY cross-peak intensities using samples prepared in 90% ^1H_2O/10% ^2H_2O or 100% ^2H_2O. In these NOESY experiments, the mixing times were arrayed (with τ_m = 48, 49, 50, 51, and 52 ms, referred to in the remainder of this paper as the τ_m = 50 ± 2 ms NOESY data sets), and the resulting spectra were added together to remove contributions from zero-quantum coherences (Macura et al., 1981). Short mixing times were used in order to minimize spin-diffusion effects. These NOESY data sets recorded with τ_m = 50 ± 2 ms were also used for quantitative estimates of many intraresidue NOEs between nonlabile protons in the sample prepared in ^2H_2O solvent.

Collection and Calibration of NOESY Data. Internuclear distance constraint lists were derived from five homonuclear and from two ^{15}N-edited NOESY data sets. These included three NOESY spectra of a hTGFα sample in 90% ^1H_2O/10% ^2H_2O recorded with mixing times τ_m = 80 and 250 ms and an array τ_m = 50 ± 2 ms. In addition, we recorded two more NOESY data sets for a sample in 100% ^2H_2O using mixing times τ_m = 100 ms and an array τ_m = 50 ± 2 ms. ^{15}N-Edited 2D HSQC–NOESY and 3D NOESY–HSQC spectra with mixing times τ_m = 80 ms were also recorded to resolve NOEs that were overlapped in the homonuclear NOESY spectrum.

Upper-bound distance constraints in the ^1H_2O spectra were calibrated using the strongest sequential $H^\alpha_i–H^N_{i+1}$ NOEs in the spectra corresponding to a distance of 2.2 Å (Billeter et al., 1982). These short distances occur in β-sheets and other extended conformations. NOESY cross peaks were used in this calibration only if the resonance of the corresponding H^α proton was greater than 0.2 ppm from the irradiated ^1H_2O resonance peak. For the data sets recorded in 100% ^2H_2O, the NOEs were calibrated by using the fixed distance of 1.8 Å between geminal glycine H^α protons. These NOEs were used as reference points for calibrating an NOE intensity (I) vs distance (d) relation, assuming that $I \propto d^{-6}$, individually for the 50 ± 2-, 80- and 100-ms NOESY spectra. Using these calibration curves, cross peaks were divided into five categories corresponding to upper-bound constraints of 2.5, 2.7, 3.0, 4.0, and 6.0 Å. The NOESY spectrum recorded with a mixing time of 250 ms in ^1H_2O was used only to verify the identities of weak cross peaks that were observed in the spectra recorded with shorter mixing times. Additional NOEs observed in the 2D and 3D ^{15}N-edited NOESY spectra were set to an upper bound of 4 Å.

When the necessary stereospecific resonance assignments were not available, pseudoatom corrections (Wüthrich et al., 1983) were added to the upper-bound distance constraints derived from the NOE data. For the case in which both NOEs between a given proton and the two protons of a single methylene group or to both methyl groups of valine and leucine could be identified, the longer of the two distance constraints was used for both methylene protons or methyl proton groups (Montelione et al., 1987, 1992).

Reiterative Evaluation of NOESY Data. The interpretation of two-dimensional NOESY data is limited by the fact that many cross peaks cannot initially be assigned to a unique pair of interacting spins because of chemical shift degeneracies. In cases where the overlaps involve amide resonances, unique assignments could generally be made using 3D ^{15}N-edited NOESY–HSQC. Degeneracies of aliphatic or aromatic resonances were overcome by reiterative evaluation of 2D NOESY spectra. In the first round of the structure calculations, 200 starting conformations with random dihedral angles were used as input for the DISMAN program (Braun & Gō, 1985), and 7 preliminary structures were computed which satisfied most of the unambiguously assigned NOEs (including 130 sequential and 131 long-range NOEs) and disulfide constraints. These structures were then used to interpret many NOESY cross peaks for which one or both ω_1 and ω_2 resonance frequencies could not be assigned unambiguously without structural information. Accordingly, these cross peaks were assigned on the basis of structural consistency. For example, consider a NOESY cross peak between resonance A and one or both of the degenerate resonances B and C. In this case, the NOE was attributed to a short distance between resonances A and B if the A–B distance was less than 5 Å and the A–C distance was greater than 6.5 Å in *all* 7 preliminary structures. If these stringent criteria were not met, the NOESY cross peak was not interpreted at this stage. The NOE constraints resulting from this reiterative interpretation procedure were then added to the upper-bound constraint list, and a new set of structures was calculated from random starting conformations. In each iteration, the constraint lists were also supplemented by the additional upper-bound contraints based on NOEs observed in the ^{15}N-edited NOESY data sets, dihedral angle constraints derived from additional scalar coupling constant measurements, and hydrogen bond constraints as described in the Results section. In this way, the NOESY spectra of hTGFα were iteratively reevaluated in five rounds of assigning NOESY cross peaks, calculating a set of structures consistent with these constraints, and using these structures to help resolve 96 ambiguities due to degeneracies of resonances.

Structure Calculation from NMR Data. Three-dimensional structures of hTGFα were computed from the NMR constraints using the DISMAN program (Braun & Gō, 1985; Braun, 1987). In this program, dihedral angle constraint violations use different units than distance constraint violations, and we used an arbitrary scaling factor of 10 for the relative weights of dihedral angle to distance constraints. The DISMAN computations were carried out on Silicon Graphics 4D-120 and 4D-240 workstations.

Evaluation of Redundant Dihedral Angle Constraints. Approximately 15% of the DISMAN calculations coverge with small residual constraint violations, which is typical of minimization calculations that suffer from the "local minimum problem" (Scheraga, 1992). Improved covergence was obtained by recalculating the structures using redundant dihedral angle constraints (REDAC) (Guntert & Wüthrich, 1991). REDACs were generated only for residues having "well-defined" local backbone conformations in all of the DISMAN structures which have low residual constraint violations. The backbone of a residue i is considered well-defined if the ϕ and ψ dihedral angles of residues $i-1$, i, and $i+1$ are confined to an area corresponding to ≤10% of the ϕ–ψ map in all of the converged DISMAN structures. A proline is well-defined if the range of ψ in all converged DISMAN structures less than 60°, since the ϕ of proline[2] is set to –75°. The largest and smallest values of ϕ_i and ψ_i in the set of 16 DISMAN structures were then used to define additional upper- and lower-bound dihedral angle constraints, a new set of starting conformations was selected randomly within the space defined by the local constraints, and a second set of hTGFα structures was calculated with the DISMAN program using the updated constraint list.

Restrained Energy Minimization. The REDAC structures were refined further by restrained energy minimization, in order to remove the most serious atomic overlaps. This was carried out as described in our earlier work on mEGF (Montelione et al., 1992) by minimizing the function $g = \alpha f + (1-\alpha)E$, where f is the sum of squares of upper, lower, and steric constraint violations, E is the ECEPP/3 energy[2] (Momany et al., 1975; Némethy et al., 1992), and α is a scaling factor between 0 and 1. Weights on peptide bond planarity constraints were adjusted so as to prevent deviations of greater than 10° from the planar trans conformation. Constraints on other dihedral angles were not considered during the energy calculations. All ionizable side chains (Asp, Glu, His, Arg) were taken to be uncharged, and no attempt was made to model the effect of solvation. These energy computations were carried out using the SUMSL minimizer (Secant unconstrained minimization solver) on an IBM 3090/600 supercomputer at the Cornell National Supercomputer Facility.

Analysis of Three-Dimensional Structures. Optimized superpositions of atomic coordinates were calculated using the algorithm of Kabsch (1978). For the statistical analyses described in this paper, "backbone atoms" refer to N, C^α, and C′ atoms. The average root-mean-squared deviations (RMSDs) among a set of structures were calculated by determining the RMSD between each pair of optimally superimposed structures in the set and then computing the average RMSD value. Molecular cartoons were drawn by using the program RIBBONS (Carson, 1991).

[2] The geometry of ECEPP/2 (Némethy et al., 1983), with ϕ_{Pro} = –75°, was used for the DISMAN calculations. ECEPP/3 (Némethy et al., 1992), with ϕ_{Pro} = –68.8° ("down" puckering), was used for the restrained energy minimization evaluations.

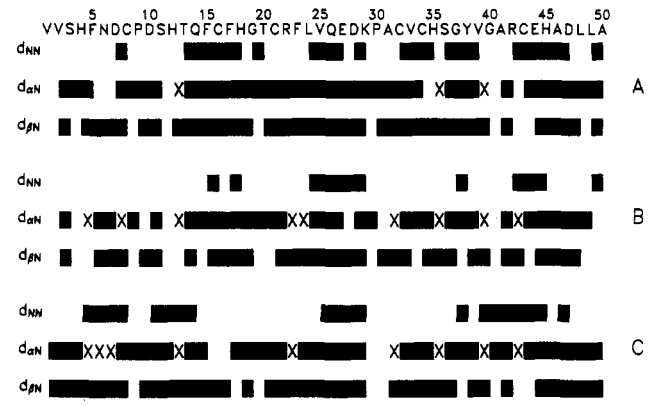

FIGURE 1: Amino acid sequence of hTGFα and summary of the sequential connectivities used in establishing the sequence-specific ^{1}H-NMR assignments. For connections involving $C^\beta H_2$ methylene groups and glycine $C^\alpha H_2$, the presence of either one or two sequential NOEs is represented by a single block. An X denotes where the expected sequential NOESY cross peaks could not be identified reliably because of chemical shift degeneracy or for other technical reasons. (A) NOEs observed for hTGFα at pH 6.5 and 10 °C. These data are from one NOESY spectrum of hTGFα in H_2O (3 mM protein concentration, τ_m = 250 ms), except for the $d_{\alpha\delta}$ NOEs of X-Pro sequences, which were determined from a sample dissolved in ^2H_2O (3 mM protein concentration, τ_m = 250 ms). (B) NOEs observed for hTGFα at pH 6.5 and 30 °C. Data are from the same samples as in (A) using a NOESY mixing time τ_m = 250 ms. (C) NOEs observed for hTGFα at pH 3.5 and 30 °C. These data are from the same NOESY spectrum of hTGFα in H_2O (4 mM protein concentration, τ_m = 200 ms), except for the $d_{\alpha\delta}$- and $d_{\beta\delta}$-type NOEs of X-Pro sequences, which were determined from a sample dissolved in ^2H_2O (2 mM protein concentration, τ_m = 200 ms).

RESULTS

Thermal Transition Detected by CD Spectroscopy. The thermal unfolding of hTGFα at pH 3.5 and 6.5 was monitored by CD spectroscopy at 202 nm. These results are shown in Figure S2 of the supplementary material. The thermal transition temperatures were 72 ± 2 and 61 ± 2 °C at pH 6.5 and 3.5, respectively. At lower pH, hTGFα also exhibits a somewhat broader thermal transition curve (supplementary Figure S2).

^{1}H and ^{15}N Resonance Assignments. Using established homonuclear and heteronuclear NMR methods, we have determined nearly complete sets of ^{1}H and ^{15}N NMR assignments for recombinant wild-type hTGFα at pH 6.5 and 10 °C, at pH 6.5 and 30 °C, and at pH 3.5 and 30 °C. Figure 1 summarizes the sequential NOE connectivities (Dubs et al., 1979; Billeter et al., 1982; Wüthrich, 1986) used to establish sequence-specific resonance assignments of hTGFα. At pH 6.5 the Cys-8–Pro-9 and Lys-29–Pro-30 peptide bonds were determined to have trans conformations from sequential NOE data (Wüthrich, 1986). At pH 3.5 the Cys-8–Pro-9 peptide bond is also trans, but the conformation of the Lys-29–Pro-30 peptide bond could not be determined unambiguously.

Some of the backbone amide resonances within the polypeptide segment Asp-10–Gly-19 are weakened in intensity by saturation transfer and intramolecular dynamical effects. In both TGFα and EGF, this portion of the polypeptide sequence adopts an irregular "loop" conformation which is attached by disulfide bonds to the core β-sheet structure. Evidence for saturation transfer and/or preirradiation-associated spin-diffusion effects to amide resonances of Thr-13 and Phe-17 was obtained at both pH 6.5 and pH 3.5 by using frequency-selective excitation experiments (Moy et al., 1992) with and without preirradiation of the H_2O solvent.

Sequence-specific ^{15}N resonance assignments were determined by combined analysis of HSQC (Figure 2) and HSQC–

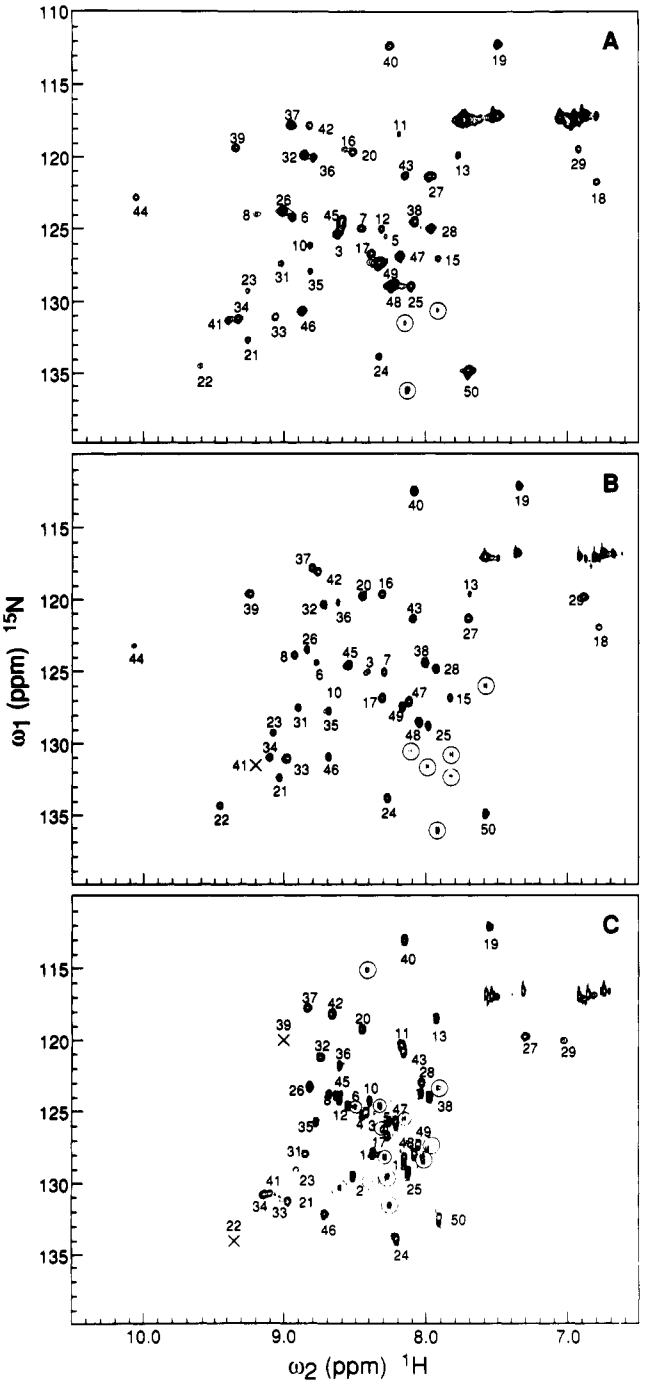

FIGURE 2: Heteronuclear single-quantum coherence (HSQC) spectra. (A) HSQC spectrum of hTGFα at pH 6.5 and 10 °C. Backbone amide ^{15}N–H^N cross peaks are labeled with their corresponding residue numbers. (B) HSQC spectrum of hTGFα at pH 6.5 and 30 °C. (C) HSQC spectrum of hTGFα at pH 3.5 and 30 °C. In all of these spectra, the locations of cross peaks that are too weak to be seen at this level of contour plotting but are observed when the data are plotted at lower contour levels are indicated by an X, and minor peaks that are not assigned are circled. Some of the side-chain amide resonances of asparagine and glutamine appearing in the spectral region (ω_1 = 116–118 ppm, ω_2 = 6.4–7.8 ppm) were also assigned but are not labeled in this figure (see supplementary Tables SI–SIII).

TOCSY (supplementary Figure S3) experiments. The HSQC spectra provided direct connectivities between amide protons and their covalently attached ^{15}N nuclei, while HSQC–TOCSY experiments provided connectivities between the ^{15}N and the H^N, H^α, H^β, and other aliphatic protons to which in-phase coherence can be transferred using isotropic mixing. Ambiguities in connecting ^{15}N resonances to assigned H^N resonances due to degeneracy of one or more H^N resonances could all be resolved by relaying the magnetization to the assigned aliphatic resonances. These assignments were corroborated in 2D HSQC–NOESY and 3D NOESY–HSQC spectra (data not shown). Nearly complete sets of ^{15}N and ^1H assignments for hTGFα at pH 6.5 and 10 °C, at pH 6.5 and 30 °C, and at pH 3.5 and 30 °C are presented in supplementary Tables SI, SII, and SIII, respectively. These backbone ^{15}N and amide proton assignments are also presented in Table I.

Table I: Backbone Amide Proton and Nitrogen-15 Assignments for hTGFα

	pH 6.5 at 10 °C		pH 6.5 at 30 °C		pH 3.5 at 30 °C	
residue	N	H^N	N	H^N	N	H^N
Val-2					129.6	8.49
Ser-3	125.3	8.59	125.1	8.40	125.2	8.40
His-4		8.50	125.1	8.53	125.1	8.43
Phe-5	125.6	8.27		8.15	125.8	8.24
Asn-6	124.2	8.92	124.4	8.78	124.7	8.53
Asp-7	125.0	8.43	125.1	8.30	123.8	8.03
Cys-8	124.0	9.18	123.9	8.91	123.9	8.66
Asp-10	126.2	8.79	125.8	8.60	124.3	8.39
Ser-11	118.4	8.16		8.05	120.4	8.14
His-12	125.0	8.33		8.26	124.3	8.57
Thr-13	119.9	7.73	119.7	7.67	118.5	7.90
Gln-14		8.57		8.42	128.0	8.35
Phe-15	127.1	7.87	126.9	7.81	128.3	8.13
Cys-16	119.5	8.56	119.7	8.33		8.18
Phe-17	126.6	8.36	126.9	8.30		8.23
His-18	121.8	6.75	121.9	6.77		
Gly-19	112.2	7.48	112.1	7.34	112.2	7.54
Thr-20	119.7	8.49	119.8	8.44	119.4	8.41
Cys-21	132.7	9.22	132.4	9.04	131.4	8.95
Arg-22	134.6	9.55	134.4	9.44	134.1	9.37
Phe-23	129.4	9.24	129.3	9.08	129.2	8.89
Leu-24	133.9	8.29	133.8	8.26	133.9	8.17
Val-25	128.9	8.07	128.8	7.97	129.3	8.11
Gln-26	123.7	8.98	123.5	8.83	123.4	8.81
Glu-27	121.4	7.95	121.3	7.69	119.9	7.24
Asp-28	125.0	7.93	124.8	7.92	123.1	7.98
Lys-29	119.5	6.89	119.8	6.87	120.2	6.98
Ala-31	127.5	9.00	127.6	8.90	128.1	8.82
Cys-32	119.9	8.83	120.4	8.71	121.3	8.72
Val-33	131.2	9.03	131.1	8.97	131.3	9.00
Cys-34	131.3	9.30	131.0	9.10		9.13
His-35	128.0	8.79	127.8	8.68	125.9	8.74
Ser-36	120.1	8.77	120.2	8.61	121.9	8.58
Gly-37	117.8	8.92	117.8	8.80	117.8	8.80
Tyr-38	124.5	8.05	124.4	8.00	124.0	7.94
Val-39	119.4	9.31	119.6	9.24	119.8	9.04
Gly-40	112.4	8.24	112.5	8.07	113.1	8.13
Ala-41	131.4	9.36	131.3	9.20	130.9	9.07
Arg-42	117.9	8.79	118.1	8.76	118.3	8.59
Cys-43	121.3	8.11	121.4	8.08	120.9	8.13
Glu-44	122.9	10.00	123.3	10.04		9.55
His-45	124.4	8.55	124.6	8.53	124.0	8.56
Ala-46	130.7	8.84	131.0	8.67	132.3	8.69
Asp-47	126.9	8.14	127.1	8.11	125.7	8.17
Leu-48	128.9	8.20	128.6	8.03	128.0	8.07
Leu-49	127.4	8.31	127.5	8.17	127.4	8.05
Ala-50	134.9	7.69	134.9	7.59	132.5	7.87

Stereospecific Assignments of $C^\beta H_2$ Methylene Protons and Valine Isopropyl Methyl Groups. Of the 50 amino acid residues in hTGFα, 36 have C^β methylene protons. Of these 36 side chains, 14 have nearly degenerate ($\Delta\delta \leq 0.1$ ppm) $C^\beta H_2$ chemical shifts or have an assignment for only one of the two $C^\beta H_2$ protons (viz., Ser-3, Asn-6, Cys-8, Asp-10, Ser-11, Phe-17, Cys-21, Arg-22, Gln-26, Glu-27, Ser-36, Glu-44, Leu-48, and Leu-49) precluding stereospecific assignment of $H^{\beta 2}$ and $H^{\beta 3}$. For 17 of the remaining 22 C^β methylenes, stereospecific H^β assignments were not obtained either because the COSY-30 cross peaks between H^α and one or both H^β's

Table II: Stereospecific $C^{\beta}H_2$ Assignments for hTGFα at pH 6.5 and 10 °C

residue	chemical shifts (ppm) H^N	H^{α}	H^{β}	$^3J_{\alpha\beta}$ (Hz)	H^N–H^{β} NOE[a]	H^{α}–H^{β} NOE[a]	χ^1 (deg)	stereospecific assignments of H^{β}
Asp-7	8.43	4.72	2.72	4	120		–60 ± 30	β3
			2.52	10	250			β2
Cys-16	8.56	4.31	2.50		130	250	60 ± 30	β3
			1.97	5	20	320		β2
Cys-32	8.83	5.40	2.79		210	180	60 ± 30	β3
			2.58	5	30	260		β2
His-35	8.79	4.88	3.40	4	100		180 ± 30	β2
			2.87	11	100			β3
His-45	8.55	5.13	3.07	4	60		–60 ± 30	β3
			2.97	10	120			β2

[a] Peak intensity in a τ_m = 50 ± 2 ms NOESY spectrum in arbitrary units.

Table III: Side-Chain Amide Proton and Nitrogen-15 Assignments for hTGFα at pH 6.5 and 10 °C

residue	proton assignments (ppm) H^{β}	H^{γ}	H^{δ}	H^{ϵ}	H^{β}–H^{δ} NOE[a]	H^{γ}–H^{ϵ} NOE[a]	stereospecific assignment	nitrogen-15 assignment (ppm)
Asn-6	2.95		7.72		100		δ2	116.3
	2.75		7.72		70			
	2.95		7.02		ovlp[c]		δ1	
	2.75		7.02		40			
Gln-14		2.17[b]		7.51		90	ε2	116.2
				6.84		50	ε1	
Gln-26		2.40[b]		7.70		90		116.5
				6.77		ovlp[c]		

[a] Peak intensity in a variable mixing time NOESY spectrum (τ_m = 50 ● 2 ms) in arbitrary units. [b] The two H^{β} protons are degenerate in chemical shift. [c] ovlp, overlap. The peak which corresponds to this NOE overlaps with another peak or is otherwise inaccessible.

were not sufficiently resolved or because the H^N–H^{β} or H^{α}–H^{β} NOEs could not be determined quantitatively. Individual $C^{\beta}H_2$ methylene protons were assigned if the combined $^3J(H^{\alpha}$–$H^{\beta})$ vicinal coupling constants, H^{α}–H^{β} NOE data, and H^N–H^{β} NOE data were consistent with one of the three staggered conformations of χ^1 = +60°, 180°, or –60°. Using these data, reliable stereospecific assignments could be made for residues Asp-7, Cys-16, Cys-32, His-35, and His-45 (Table II) which appear to adopt staggered rotamer states in hTGFα at pH 6.5.

On the basis of intraresidue NOEs with H^N and H^{α}, the upfield and downfield methyl resonances of Val-25 were assigned at pH 6.5 as $C^{\gamma 1}H_3$ and $C^{\gamma 2}H_3$, respectively, and χ^1 was found to be +60 ± 30°. Stereospecific assignments for the Val-39 and Val-33 isopropyl methyl groups could not be made because of resonance overlap. The H^N resonance of Val-2 has not been assigned at pH 6.5, preventing a determination of stereospecific assignments for its isopropyl methyl group.

Individual Assignments of Side-Chain Amide Protons. hTGFα has one asparagine and two glutamine residues. The nitrogen-15 resonance assignments for these three side-chain amide resonances are listed in Table III. Individual assignments for the side-chain amide proton resonances of Asn-6 and Gln-14 at pH 6.5, and the NOE data upon which these assignments are based, are also presented in Table III. It was not possible to obtain unique assignments for the side-chain amide protons of Gln-26 due to overlaps between NOESY cross peaks.

Experimental Conformational Constraints. Structures of hTGFα were calculated from NMR data obtained at pH 6.5 and a temperature of 10 °C. Five kinds of experimental constraints were used in the input: (i) NOE-derived upper-bound ^1H–^1H distance constraints; (ii) constraints on ranges of backbone dihedral angles from vicinal $^3J(H^N$–$H^{\alpha})$ coupling constants and from REDAC analysis; (iii) constraints on ranges of side-chain dihedral angles χ^1 determined by combined analysis of COSY-30 and NOESY data; (iv) constraints associated with hydrogen bonds that were characterized by slow amide exchange at pH 3.5 and 30 °C and were consistent with NOE patterns and $^3J(H^N$–$H^{\alpha})$ coupling constants at pH 6.5; (v) disulfide bond constraints. A complete list of the conformational constraints used as input in these structure calculations has been deposited in the Brookhaven Protein Data Bank, together with the atomic coordinates.

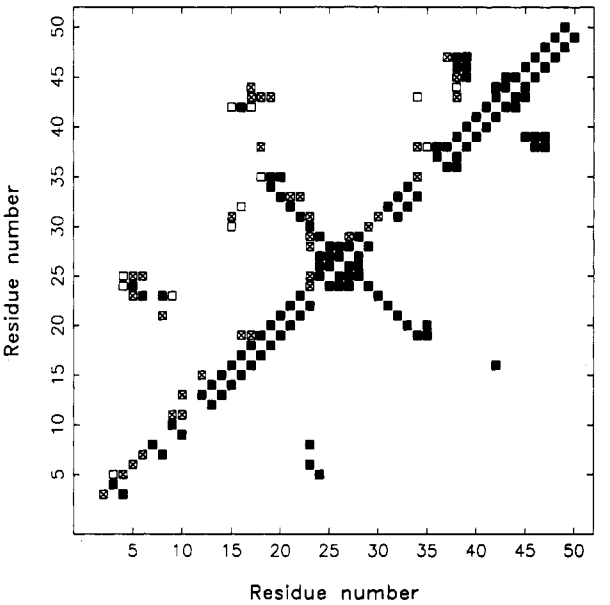

FIGURE 3: Survey of NOE-derived distance constraints for hTGFα at pH 6.5 and 10 °C. Each axis is labeled with the amino acid sequence numbers of hTGFα. Solid, crossed, and open squares at coordinate *i*, *j* indicate that one or more backbone to backbone, backbone to side-chain, or side-chain to side-chain NOEs, respectively, have been identified between atoms of residues *i* and *j*.

The NOE-derived upper-bound distance constraints were obtained as described in the Materials and Methods section. Altogether, 58 intraresidue, 130 sequential, and 169 long-

Table IV: Experimental Values of $^3J(H^N–H^\alpha)$ Coupling Constants Measured by 2D HSQC-J

residue	pH 6.5 at 10 °C (Hz)	pH 6.5 at 30 °C (Hz)	pH 3.5 at 30 °C (Hz)
Val-2			7.5 ± 0.5
Ser-3	7.0 ± 1.0	7.5 ± 1.5	
Phe-5	7.5 ± 0.5		7.5 ± 0.5
Asn-6	8.0 ± 2.0	9.0 ± 1.0	
Asp-7	5.5 ± 1.5	6.0 ± 1.0	7.0 ± 1.0
Cys-8	<9.0	5.5 ± 1.5	5.5 ± 1.5
Asp-10	<5.0	<6.0	
Ser-11	<8.0		6.5 ± 0.5
His-12	8.0 ± 2.0		
Thr-13	<5.0	<6.0	8.5 ± 0.5
Gln-14			6.5 ± 0.5
Phe-15	<7.0	5.0 ± 1.0	6.5 ● 0.5
Cys-16	<10.0	8.5 ± 0.5	
Phe-17	6.0 ± 1.0	6.5 ± 0.5	7.0 ± 1.0
Thr-20	9.0 ● 1.0	9.5 ± 0.5	9.0 ± 1.0
Cys-21	<7.0	6.0 ± 1.0	<9.0
Arg-22	9.0 ± 1.0	9.0 ± 1.0	
Phe-23	<9.0	8.0 ± 1.0	
Leu-24	7.0 ± 2.0	8.0 ± 1.0	8.5 ± 0.5
Val-25	5.0 ± 1.0	<4.0	5.0 ● 1.0
Gln-26	<6.0	5.0 ± 0.1	5.0 ± 1.0
Glu-27	7.0 ± 1.0	8.0 ± 1.0	
Asp-28	7.0 ± 1.0	7.5 ± 0.5	7.0 ± 1.0
Lys-29	<8.0	7.5 ± 0.5	
Ala-31	<10.0	8.5 ± 0.5	
Cys-32	9.0 ± 1.0	9.5 ± 0.5	>8.0
Val-33	9.0 ± 1.0	9.5 ± 0.5	<9.0
Cys-34	<5.0	4.5 ± 1.5	<9.0
His-35	<9.0	6.0 ± 1.0	5.0 ± 1.0
Ser-36	<4.0	<4.0	<4.0
Tyr-38	9.0 ± 1.0	9.5 ± 0.5	9.5 ± 0.5
Val-39	9.0 ± 1.0	9.0 ± 1.0	
Ala-41	<6.0	<9.0	<9.0
Arg-42	9.0 ± 1.0	9.5 ± 0.5	>8.0
Cys-43	<6.0	6.5 ± 0.5	
Glu-44	<8.0		
His-45	8.0 ± 1.0	9.5 ± 0.5	9.0 ± 1.0
Ala-46	<6.0	6.0 ± 1.0	6.0 ± 2.0
Asp-47	6.5 ± 0.5	6.5 ± 0.5	7.5 ± 0.5
Leu-48	6.5 ± 0.5	7.0 ± 1.0	7.5 ± 0.5
Leu-49	7.5 ± 0.5	8.0 ± 1.0	7.5 ● 0.5
Ala-50	6.5 ± 0.5	6.5 ± 0.5	6.5 ± 0.5

range conformation-dependent NOE constraints were extracted from the NOESY data set. The distribution of NOE-derived upper-bound distance constraints (Figure 3) indicates that the hTGFα structure is divided into two slightly overlapping subdomains corresponding to residues 1–35 and 34–50, respectively. The relative orientation of these two subdomains is determined by 32 NOE-derived constraints between the polypeptide segments Phe-15–Gly-19 and Tyr-38–Glu-44 and by the backbone conformation of the "hinge region" polypeptide segment Cys-32–Tyr-38. The interactions between these domains include side-chain to side-chain, side-chain to backbone, and one backbone to backbone NOE (Figure 3).

In hTGFα, most $^3J(H^N–H^\alpha)$ coupling constants cannot be measured reliably from 2QF-COSY spectra because of line broadening. Accordingly, the HSQC-J experiment (Neri et al., 1990; Billeter et al., 1992) with incremented delays τ was used to obtain reliable estimates of $^3J(H^N–H^\alpha)$ coupling constants. A summary of $^3J(H^N–H^\alpha)$ coupling constants measured by HSQC-J under the three conditions of pH and temperature described above is presented in Table IV. Fifteen $^3J(H^N–H^\alpha)$ coupling constants ≥8 Hz were measured at pH 6.5, including those of residues Asn-6, His-12, Cys-16, Thr-20, Arg-22, Phe-23, Leu-24, Glu-27, Ala-31, Cys-32, Val-33, Tyr-38, Val-39, Arg-42, and His-45. Accordingly, the backbone dihedral angles ϕ of these residues were initially

Table V: Redundant Dihedral Angle Constraints on ϕ and ψ of hTGFα at pH 6.5 and 10 °C

residue	ϕ_{min}	ϕ_{max}	ψ_{min}	ψ_{max}	fractional area of ϕ–ψ space
His-18[a]	−148	175	58	92	0.0349
Gly-19	−167	−126	−143	178	0.0444
Thr-20	−123	−73	90	161	0.0908
Cys-21	−145	−72	124	146	0.0446
Arg-22	−162	−141	88	157	0.0402
Phe-23	−135	−88	111	132	0.0274
Leu-24	−108	−75	67	95	0.0257
Val-25	−60	−37	−52	−34	0.0115
Gln-26	−58	−38	−46	−18	0.0156
Glu-27	−137	−90	−19	22	0.0535
Asp-28[a]	28	66	12	72	0.0633
Pro-30[a]	−75	−75	116	153	*b*
Ala-31	−162	−135	85	146	0.0458
Cys-32[a]	−129	−95	−168	135	0.0538

[a] These residues were not used in REDAC calculations because one neighboring residue was not constrained to <10% of the ϕ–ψ map in the set of DISMAN structures. [b] Fractional areas are not reported for proline residues because the dihedral angle ϕ is fixed at −75° in DISMAN.

constrained to the range −120 ± 40°. For residues Val-25 and Ser-36, $^3J(H^N–H^\alpha)$ < 4 Hz restricting the backbone conformation of these residues to the range $-70° < \phi < 180°$. Backbone dihedral angle constraints were also determined for residues Gly-19, Cys-21, and Gln-26 from the REDAC analysis summarized below. In addition, constraints on the ranges of five side-chain dihedral angles χ^1 were determined from the data summarized in Table II, and dihedral angle χ^1 of residue Val-25 was constrained to +60 ± 30° from NOE measurements.

Interstrand hydrogen bonds in the β-sheet structures were located by identifying slowly exchanging amide protons of hTGFα at pH 3.5 and 30 °C (Brown et al., 1989; Montelione et al., 1989). These hydrogen bonds were used as constraints for the structure determination at pH 6.5 if they were consistent with the NOE patterns and $^3J(H^N–H^\alpha)$ values at pH 6.5 and if they were in regions of the backbone structure demonstrated to be unaltered by this pH difference, as discussed below. The following six hydrogen-bonded pairs were identified on this basis: Thr-20 HN–Val-33 O, Thr-20 O–Val-33 HN, Arg-22 HN–Ala-31 O, Arg-22 O–Ala-31 HN, Leu-24 HN–Lys-29 O, and Val-39 HN–His-45 O. One of these hydrogen-bonded pairs, Thr-20 HN–Val-30 O, was not observed by Montelione et al. (1989) but was identified as slowly exchanging by Kline et al. (1989). Upper- and lower-bound H^N–O and N–O distance constraints for each of these six hydrogen bonds, as well as S–S and C^β–S distance constraints which fix bond lengths and bond angles in the three disulfide bonds (Winkler et al., 1986), were defined as described elsewhere (Williamson et al., 1985; Wüthrich, 1986). In summary, for calculations of the final structures used to represent the solution conformations of hTGFα, 425 conformational constraints were used, including 357 NOE-derived upper-bound distance constraints, 26 dihedral angle constraints, and 42 upper- and lower-bound distances associated with six hydrogen bonds and three disulfide bonds.

Determination of the Solution Structure at pH 6.5. For each residue along the polypeptide chain, ranges of ϕ, ψ, and χ^1 consistent with the local NOE and scalar coupling constant data were determined. A total of 200 starting conformations of the entire 50-residue hTGFα molecule were then generated with values for the dihedral angles selected randomly within these allowed ranges. All peptide bonds were kept fixed in the planar trans conformation. Of the resulting 200 structures,

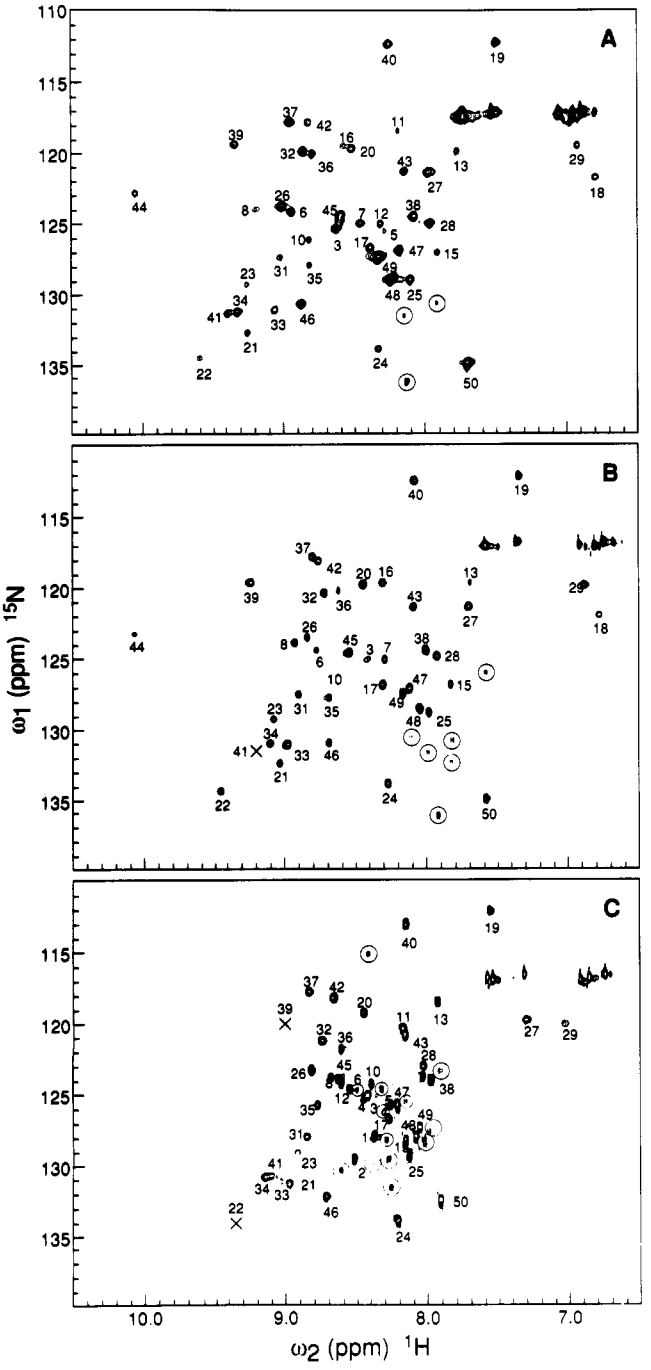

FIGURE 2: Heteronuclear single-quantum coherence (HSQC) spectra. (A) HSQC spectrum of hTGFα at pH 6.5 and 10 °C. Backbone amide ^{15}N–H^N cross peaks are labeled with their corresponding residue numbers. (B) HSQC spectrum of hTGFα at pH 6.5 and 30 °C. (C) HSQC spectrum of hTGFα at pH 3.5 and 30 °C. In all of these spectra, the locations of cross peaks that are too weak to be seen at this level of contour plotting but are observed when the data are plotted at lower contour levels are indicated by an X, and minor peaks that are not assigned are circled. Some of the side-chain amide resonances of asparagine and glutamine appearing in the spectral region (ω_1 = 116–118 ppm, ω_2 = 6.4–7.8 ppm) were also assigned but are not labeled in this figure (see supplementary Tables SI–SIII).

TOCSY (supplementary Figure S3) experiments. The HSQC spectra provided direct connectivities between amide protons and their covalently attached ^{15}N nuclei, while HSQC–TOCSY experiments provided connectivities between the ^{15}N and the H^N, H^α, H^β, and other aliphatic protons to which in-phase coherence can be transferred using isotropic mixing. Ambiguities in connecting ^{15}N resonances to assigned H^N resonances due to degeneracy of one or more H^N resonances could all be resolved by relaying the magnetization to the assigned aliphatic resonances. These assignments were corroborated in 2D HSQC–NOESY and 3D NOESY–HSQC spectra (data not shown). Nearly complete sets of ^{15}N and ^1H assignments for hTGFα at pH 6.5 and 10 °C, at pH 6.5 and 30 °C, and at pH 3.5 and 30 °C are presented in supplementary Tables SI, SII, and SIII, respectively. These backbone ^{15}N and amide proton assignments are also presented in Table I.

Table I: Backbone Amide Proton and Nitrogen-15 Assignments for hTGFα

	pH 6.5 at 10 °C		pH 6.5 at 30 °C		pH 3.5 at 30 °C	
residue	N	H^N	N	H^N	N	H^N
Val-2					129.6	8.49
Ser-3	125.3	8.59	125.1	8.40	125.2	8.40
His-4		8.50	125.1	8.53	125.1	8.43
Phe-5	125.6	8.27		8.15	125.8	8.24
Asn-6	124.2	8.92	124.4	8.78	124.7	8.53
Asp-7	125.0	8.43	125.1	8.30	123.8	8.03
Cys-8	124.0	9.18	123.9	8.91	123.9	8.66
Asp-10	126.2	8.79	125.8	8.60	124.3	8.39
Ser-11	118.4	8.16		8.05	120.4	8.14
His-12	125.0	8.33		8.26	124.3	8.57
Thr-13	119.9	7.73	119.7	7.67	118.5	7.90
Gln-14		8.57		8.42	128.0	8.35
Phe-15	127.1	7.87	126.9	7.81	128.3	8.13
Cys-16	119.5	8.56	119.7	8.33		8.18
Phe-17	126.6	8.36	126.9	8.30		8.23
His-18	121.8	6.75	121.9	6.77		
Gly-19	112.2	7.48	112.1	7.34	112.2	7.54
Thr-20	119.7	8.49	119.8	8.44	119.4	8.41
Cys-21	132.7	9.22	132.4	9.04	131.4	8.95
Arg-22	134.6	9.55	134.4	9.44	134.1	9.37
Phe-23	129.4	9.24	129.3	9.08	129.2	8.89
Leu-24	133.9	8.29	133.8	8.26	133.9	8.17
Val-25	128.9	8.07	128.8	7.97	129.3	8.11
Gln-26	123.7	8.98	123.5	8.83	123.4	8.81
Glu-27	121.4	7.95	121.3	7.69	119.9	7.24
Asp-28	125.0	7.93	124.8	7.92	123.1	7.98
Lys-29	119.5	6.89	119.8	6.87	120.2	6.98
Ala-31	127.5	9.00	127.6	8.90	128.1	8.82
Cys-32	119.9	8.83	120.4	8.71	121.3	8.72
Val-33	131.2	9.03	131.1	8.97	131.3	9.00
Cys-34	131.3	9.30	131.0	9.10		9.13
His-35	128.0	8.79	127.8	8.68	125.9	8.74
Ser-36	120.1	8.77	120.2	8.61	121.9	8.58
Gly-37	117.8	8.92	117.8	8.80	117.8	8.80
Tyr-38	124.5	8.05	124.4	8.00	124.0	7.94
Val-39	119.4	9.31	119.6	9.24	119.8	9.04
Gly-40	112.4	8.24	112.5	8.07	113.1	8.13
Ala-41	131.4	9.36	131.3	9.20	130.9	9.07
Arg-42	117.9	8.79	118.1	8.76	118.3	8.59
Cys-43	121.3	8.11	121.4	8.08	120.9	8.13
Glu-44	122.9	10.00	123.3	10.04		9.55
His-45	124.4	8.55	124.6	8.53	124.0	8.56
Ala-46	130.7	8.84	131.0	8.67	132.3	8.69
Asp-47	126.9	8.14	127.1	8.11	125.7	8.17
Leu-48	128.9	8.20	128.6	8.03	128.0	8.07
Leu-49	127.4	8.31	127.5	8.17	127.4	8.05
Ala-50	134.9	7.69	134.9	7.59	132.5	7.87

Stereospecific Assignments of $C^\beta H_2$ Methylene Protons and Valine Isopropyl Methyl Groups. Of the 50 amino acid residues in hTGFα, 36 have C^β methylene protons. Of these 36 side chains, 14 have nearly degenerate ($\Delta\delta \leq 0.1$ ppm) $C^\beta H_2$ chemical shifts or have an assignment for only one of the two $C^\beta H_2$ protons (viz., Ser-3, Asn-6, Cys-8, Asp-10, Ser-11, Phe-17, Cys-21, Arg-22, Gln-26, Glu-27, Ser-36, Glu-44, Leu-48, and Leu-49) precluding stereospecific assignment of $H^{\beta 2}$ and $H^{\beta 3}$. For 17 of the remaining 22 C^β methylenes, stereospecific H^β assignments were not obtained either because the COSY-30 cross peaks between H^α and one or both H^β's

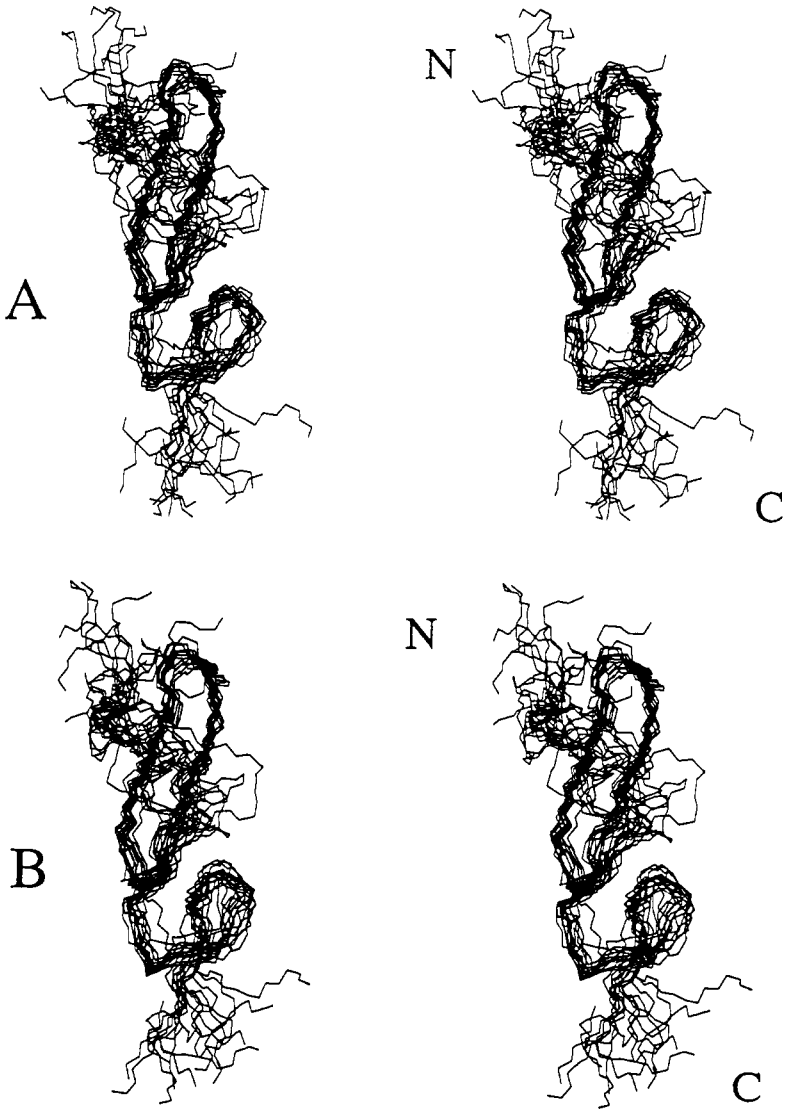

FIGURE 4: Stereo diagrams showing superpositions of the polypeptide backbone atoms (N, C^{α}, C′) of polypeptide segment Phe-5–Asp-47 at pH 6.5 and 10 °C. (A) Sixteen REDAC conformers. (B) Fifteen ECEPP conformers. Each set of superpositions was generated using conformer 1 (Table VI) as the reference and orienting the other conformers so as to minimize the pairwise RMSD for these backbone atoms. The N- and C-termini are labeled.

minimization were carried out as follows. (i) The restrained energy function g was minimized with $\alpha = 0.9900$. (ii) In 6 of the 16 minimized conformations from step i, χ^4 of Gln-14 was close to 0° rather than 180°. Since this interchanges the $H^{\epsilon 1}$ and $H^{\epsilon 2}$ atoms and thus compromises the NOE assignments involving the $H^{\epsilon 1}$ and $H^{\epsilon 2}$ atoms, χ^4 of Gln-14 was adjusted by adding 180° in those conformations. The restrained energy function g was then minimized again, with $\alpha = 0.9890$, starting from the (adjusted) dihedral angles from step i. (iii) The dihedral angles from step ii were used as starting points for minimization of the function g with $\alpha = 0.9875$. (iv) The dihedral angles from step iii were used as starting points for minimization of the function g with $\alpha = 0.9860$. At this stage 15 of 16 conformers had negative energies. (v) Finally, the dihedral angles from step iv were used as starting points for minimization of the function g with $\alpha = 0.9800$. Further minimization of the energies of these structures with smaller values of α resulted in significant residual constraint violations.

All violations of lower-bound constraints and appoximately half of the steric overlaps exceeding 0.3 Å were removed in the first step of the energy refinement, but the number of dihedral angle constraint violations was increased. This is understandable since constraints on dihedral angles were not

Table VII: Comparison of the 16 hTGFα Conformers of Table VI Used To Represent the Solution Structure

	mean RMSD	
polypeptide segment[a]	backbone atoms[b]	heavy atoms[c]
Phe-15–Cys-34 (A)	1.07(0.91–1.43)	2.05(1.88–2.49)
Phe-15–Cys-34 (B)	0.86(0.75–1.08)	1.93(1.75–2.25)
Phe-15–Cys-34 (C)	0.97(0.83–1.15)	1.97(1.77–2.28)
Phe-15–Cys-34 (D)	0.42	0.63
Val-33–Asp-47 (A)	1.35(1.13–1.62)	2.22(2.03–2.75)
Val-33–Asp-47 (B)	1.26(1.10–1.78)	2.06(1.86–2.41)
Val-33–Asp-47 (C)	1.28(1.07–1.59)	2.10(1.87–2.30)
Val-33–Asp-47 (D)	0.39	0.72
Phe-15–Asp-47 (A)	1.58(1.34–1.95)	2.45(2.27–2.92)
Phe-15–Asp-47 (B)	1.51(1.29–2.05)	2.36(2.22–2.73)
Phe-15–Asp-47 (C)	1.59(1.34–1.91)	2.39(2.21–2.62)
Phe-15–Asp-47 (D)	0.66	0.81

[a] A, DISMAN structures; B, REDAC structures; C, ECEPP structures; D, comparison of averaged REDAC and averaged ECEPP structures. [b] Average (range) RMSDs calculated for the N, C^{α}, and C′ backbone atoms for all pairwise combinations of the 16 DISMAN, 16 REDAC, and 15 ECEPP structures. [c] Average (range) RMSDs calculated for the heavy atoms for all pairwise combinations of the 16 DISMAN, 16 REDAC, and 15 ECEPP structures.

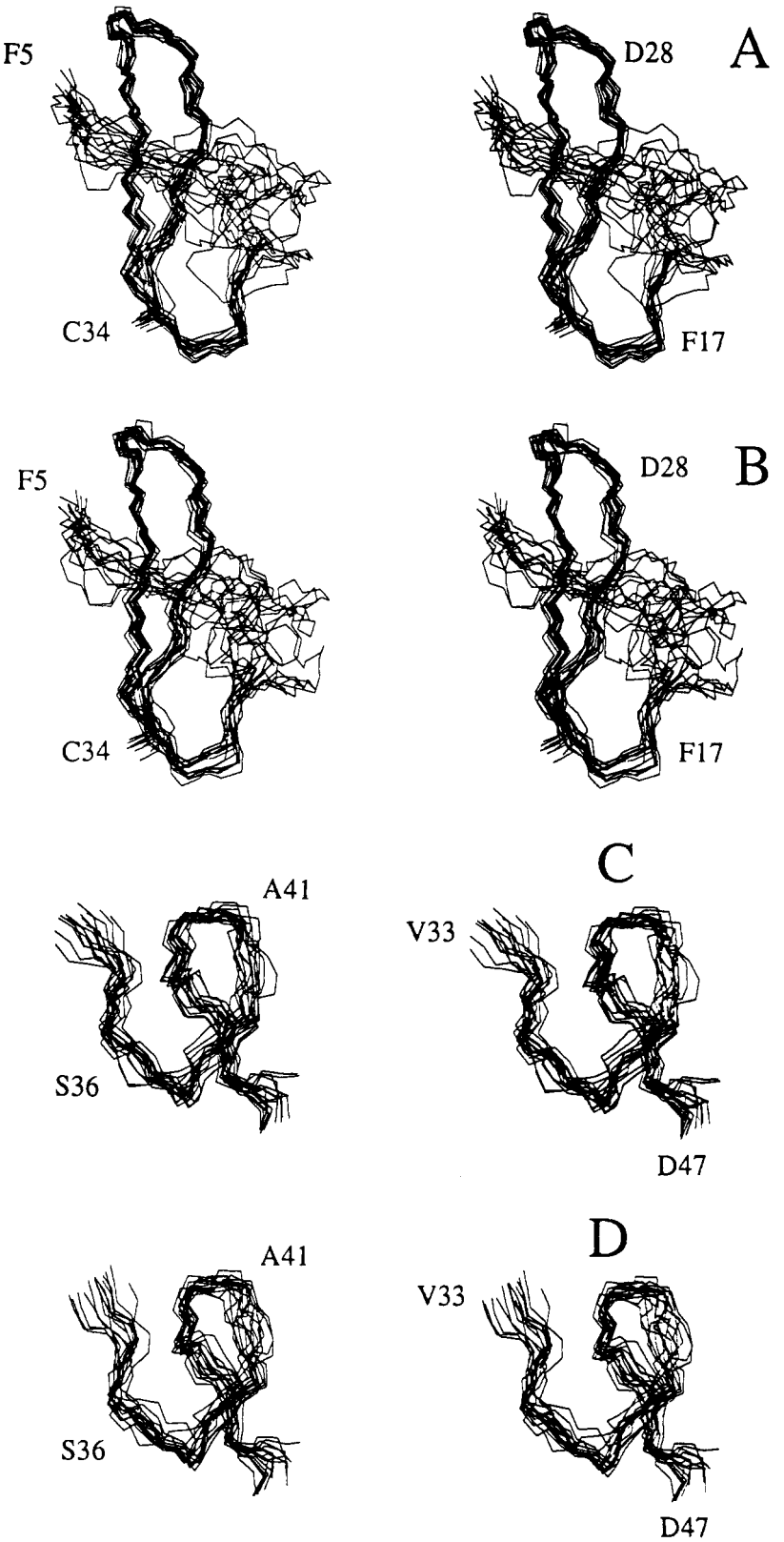

FIGURE 5: Stereo diagrams showing superpositions of the backbone atoms (N, C^{α}, C') of polypeptide segments Phe-5–Cys-34 and Val-33–Asp-47 at pH 6.5 and 10 °C. (A) Residues Phe-5–Cys-34, 16 REDAC conformers. (B) Residues Phe-5–Cys-34, 15 ECEPP conformers. (C) Residues Val-33–Asp-47, 16 REDAC conformers. (D) Residues Val-33–Asp-47, 15 ECEPP conformers. Each set of superpositions was generated using conformer 1 (Table VI) as a reference and orienting the other conformers so as to minimize the RMSD for these backbone atoms.

considered in the restrained energy refinement. Four structures, **1**, **10**, **14**, and **16**, still had positive ECEPP/3 energies at this stage. By the end of step ii, the ECEPP/3 energy had decreased further without significantly affecting the constraint violations. After step iii, only structures **14** and **16** still had positive ECEPP/3 energies, and the number of constraint violations was essentially unchanged. At the end of step iv, only structure **14** still had a positive value of the ECEPP/3 energy. However, at this stage the number of upper-bound constraint violations had begun to increase. At the end of step v the number of both upper-bound and steric constraint violations had increased still further. Accordingly, structural

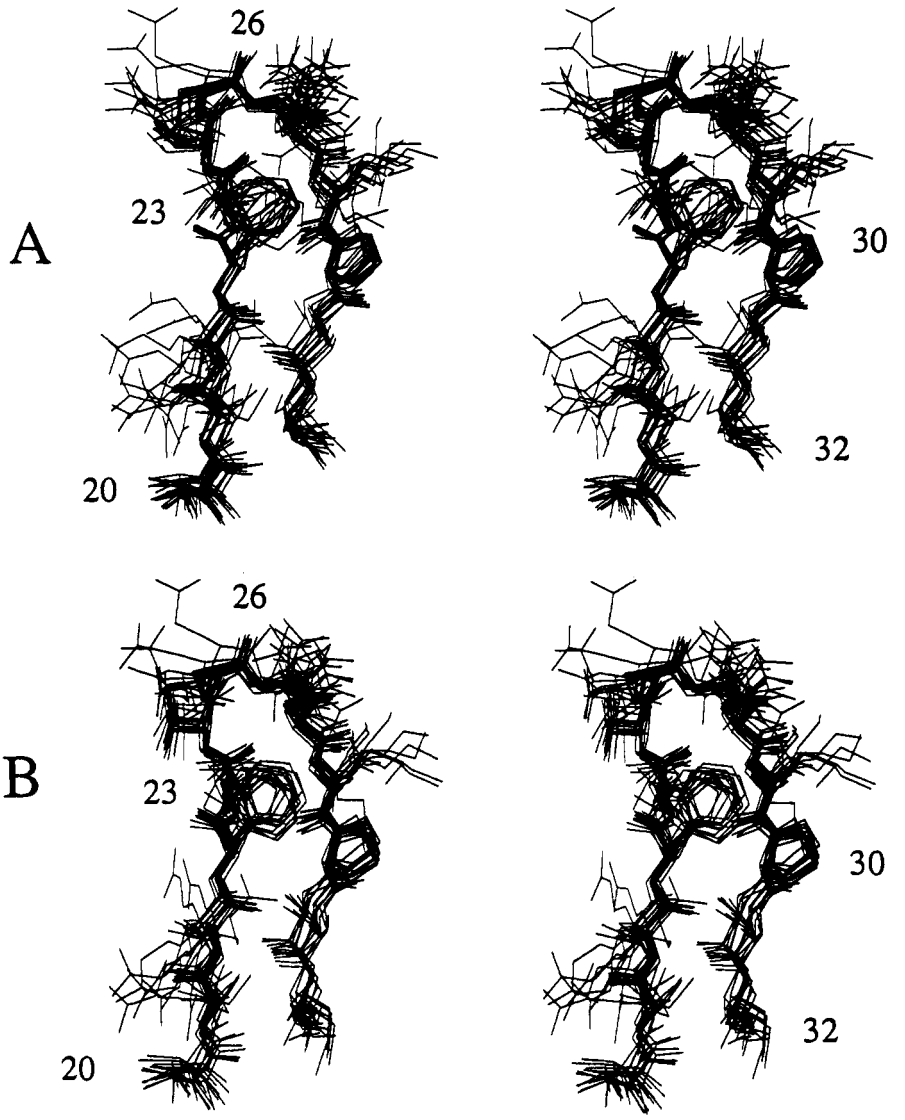

FIGURE 6: Stereo diagrams showing superpositions for all heavy atoms of the polypeptide segment Thr-20–Cys-32 of hTGFα at pH 6.5 and 10 °C. (A) Sixteen REDAC conformers. (B) Fifteen ECEPP conformers.

analysis was carried out on the conformations obtained at the end of step iv, which are referred to here as the "ECEPP structures".

A summary of the residual constraint violations and conformational energies of the final 16 hTGFα structures after DISMAN, REDAC analysis followed by DISMAN, and restrained energy minimization is presented in Table VI. There are an average of 0.14 and 3.9 violations of upper-bound constraints greater than 1 Å, and between 0.5 and 1.0 Å, respectively, in each of the 16 energy-refined structures. The two upper-bound violations greater than 1 Å correspond to NOEs between Asp-47 H^{α} with Leu-48 H^{N} and Thr-20 H^{β} with Val-33 H^{β}.

ECEPP/3 minimization lowered the potential energies of REDAC structures significantly without seriously violating the experimental constraints (Table VI). All of these energy-refined structures have negative values of the ECEPP/3 energy except structure **14**. For this reason, structure **14** was not used in further statistical analyses.

Analysis of Solution Structures of hTGFα. Superpositions of backbone atoms for the 16 REDAC and 15 ECEPP structures are shown in Figure 4, and statistics for the superpositions of backbone and heavy atoms for the DISMAN, REDAC, and ECEPP structures are presented in Table VII. Residues 1–14 and 48–50 are not well-defined (Figure 4). For residues 15–47, the average pairwise RMSDs for N, C^{α}, and C′ atoms are 1.5 and 1.6 Å for REDAC and ECEPP structures, respectively. For the same set of residues, the corresponding average RMSD values for *all* heavy (C, N, O, and S) atoms are 2.4 Å for both the REDAC and ECEPP structures.

The quality of the structure determination within the N-terminal and C-terminal subdomains is better than for the overall molecule. For the polypeptide segments Phe-15–Cys-34 and Val-33–Asp-47 the averaged backbone RMSDs of the REDAC (0.9 and 1.3 Å, respectively) or ECEPP (1.0 and 1.3 Å, respectively) structures are significantly lower than the corresponding values for the entire segment of residues Phe-15–Asp-47 (1.5 Å for REDAC structures and 1.6 Å for ECEPP structures). Similar results were obtained in the structure calculations of murine EGF (Montelione et al., 1992). Stereo diagrams showing superpositions of the backbone atoms for the two subdomains of hTGFα are shown in Figure 5.

Many residues also have reasonably well determined side-chain conformations. Superpositions of heavy atom coordinates for polypeptide segments Phe-15–Cys-34 and Val-33–Asp-47 have RMSDs of about 2 Å in the REDAC and ECEPP structures (Table VII). Stereo diagrams showing superpositions of heavy atom coordinates for the polypeptide segment Thr-20–Cys-32 of the 16 REDAC and 15 ECEPP structures are shown in Figure 6. Stereo diagrams of complete heavy

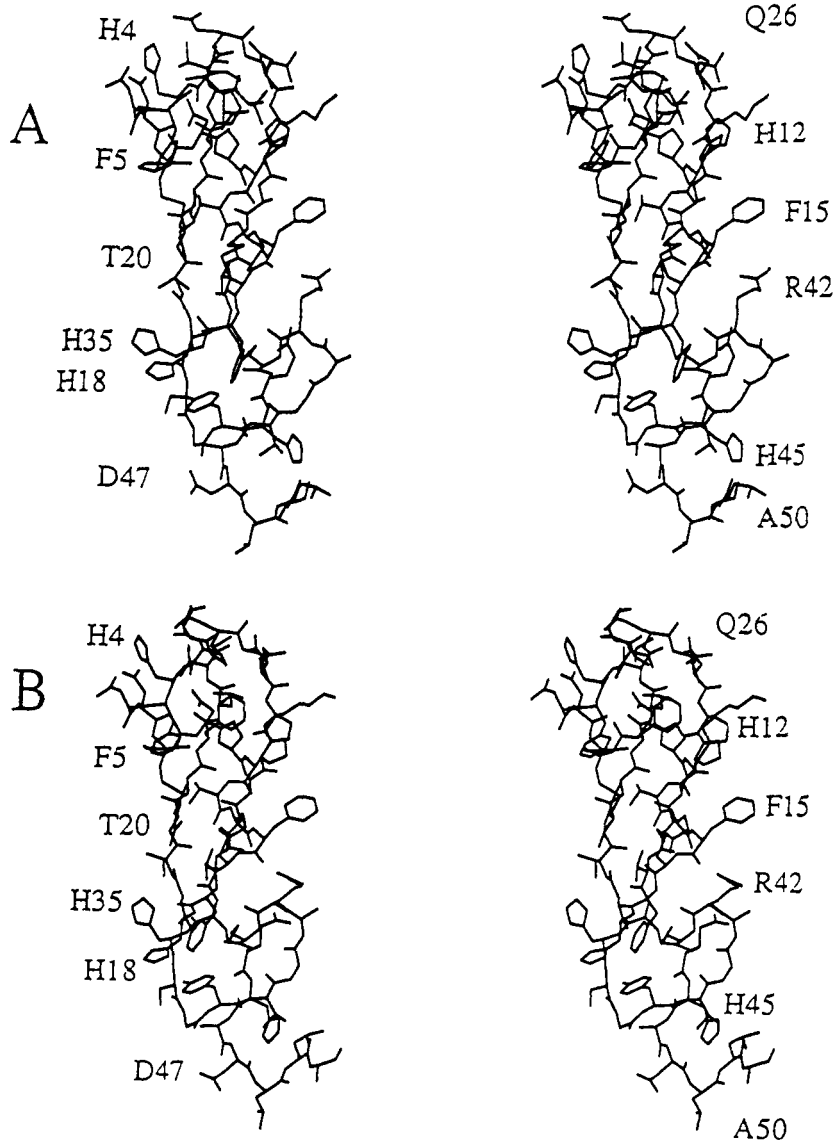

FIGURE 7: Stereo diagrams of conformer 1 (Table VI) of hTGFα showing all heavy atoms. (A) REDAC conformer. (B) ECEPP conformer, oriented so as to minimize the RMSD for the backbone atoms of residues Phe-5–Asp-47 with respect to the REDAC conformer in panel A.

atom coordinates for one REDAC and one ECEPP structure are shown in Figure 7.

While the restrained energy minimization relieved many high-energy interactions, it did not significantly alter the three-dimensional structure of hTGFα. The RMSDs between the averaged backbone coordinates of the REDAC and ECEPP hTGFα structures are 0.7, 0.4, and 0.4 Å for residues 15–47, 15–34, and 33–47, respectively. Similar results were obtained in comparisons of the heavy atom coordinates (Table VII).

Composite ϕ–ψ plots of the DISMAN, REDAC, and energy-refined structures are shown in Figure 8. These ϕ–ψ plots provide a useful tool for evaluating the quality of a protein structure determination since amino acid residues in proteins generally adopt backbone conformations corresponding to low-energy minima of amino acid residues in small peptides (Ramachandran & Sasisekharan, 1968; Roterman et al., 1989). The ϕ–ψ plots shown in Figure 8 reveal convergence in low-energy regions of conformational space in the successive stages of the refinement procedure.

As shown in the ϕ–ψ plots of Figure 8, most non-glycine residues have negative values of the dihedral angle ϕ, which is typical for L-amino acids in proteins. However, positive ϕ values for non-glycine residues are also observed in some parts of these hTGFα structures, even after energy minimization. The incidences of these positive ϕ values are summarized in Table VIII. Residues Asp-28, Gly-37, and Cys-43 have positive ϕ values in nearly all of the ECEPP structures. These three residues occur in various bend conformations in hTGFα. They also have positive ϕ values in the homologous structure of murine EGF (Montelione et al., 1992). Other residues that have positive ϕ values in some of the ECEPP structures of hTGFα include Phe-15, Gly-19, His-35, Ser-36, Gly-40, Ala-41, Arg-42, and Asp-47 (Table VIII). For most of these residues, the available NMR data are not sufficient to distinguish positive and negative values of the ϕ dihedral angle since the measured values of the corresponding $^3J(H^N–H^\alpha)$ coupling constants are <8 Hz. However, for residue Arg-42 the measured value of $^3J(H^N–H^\alpha)$ is 9 ± 1 Hz, which is inconsistent with a positive value of ϕ.

Comparison of Structural Parameters for hTGFα at Neutral and Acidic pH. A pH-induced disordering of the first strand of the N-terminal β-sheet was evident from an analysis of interstrand NOEs at pH 6.5 and 3.5. NOESY cross peaks are observed between the resonances Phe-5 H^α and Leu-24 H^α at both 10 and 30 °C at pH 6.5. An NOE is also observed between Asn-6 H^N and Phe-23 H^N at pH 6.5 and 10 °C. These two backbone–backbone NOEs and other NOEs involving side-chain protons of polypeptide segments

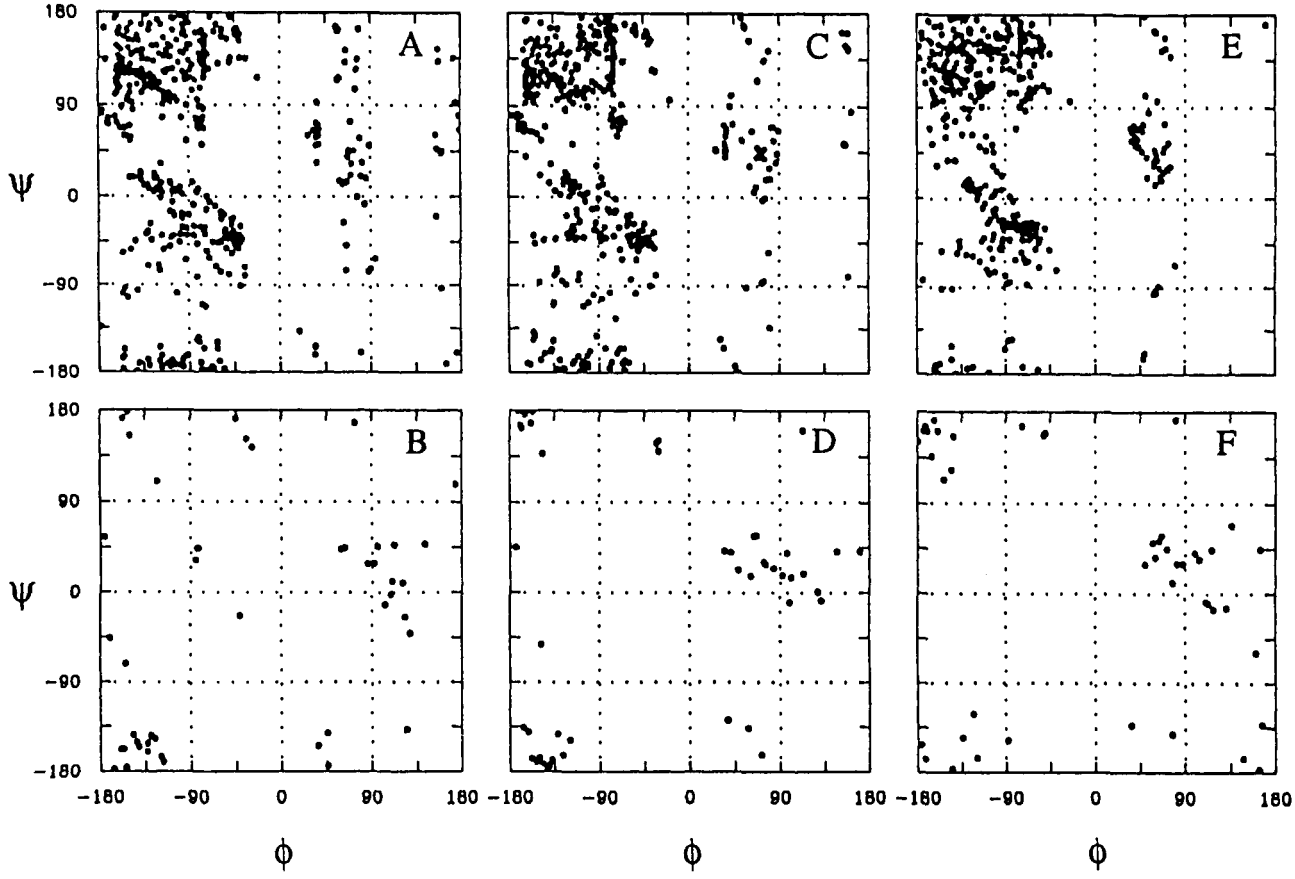

FIGURE 8: Composite ϕ–ψ map for residues Phe-15–Asp-47 of hTGFα at pH 6.5 and 10 °C. (A) Non-glycine residues for 16 DISMAN conformers. (B) Glycine residues for 16 DISMAN conformers. (C) Non-glycine residues for 16 REDAC conformers. (D) Glycine residues for 16 REDAC conformers. (E) Non-glycine residues for 15 ECEPP conformers. (F) Glycine residues for 15 ECEPP conformers.

Table VIII: Incidence of Positive Dihedral Angles ϕ in hTGFα Structures at pH 6.5 and 10 °C

	no. of conformations for which $\phi > 0°$		
residue[a]	16 DISMAN structures	16 REDAC structures	15 ECEPP structures[b]
Phe-15	4	7	7
His-18	3	1	0
Gly-19	0	0	1
Asp-28	16	15	14
Cys-34	1	1	0
His-35	2	1	1
Ser-36	11	11	6
Gly-37	13	16	15
Gly-40	6	6	9
Ala-41	4	6	5
Arg-42	3	2	2
Cys-43	16	16	14
Glu-44	2	0	0
Asp-47	4	4	3

[a] Positive ϕ values are summarized for the polypeptide segment Phe-15–Asp-47 only, since the backbone conformations of residues outside of this segment are not well-defined. [b] The one ECEPP structure with a positive value of the ECEPP/3 energy was not included in this analysis.

His-4–Asn-6 and Phe-23–Val-25 provide evidence for a loosely attached first strand of the N-terminal β-sheet at pH 6.5. However, these NOEs are not observed in the spectra recorded at pH 3.5.

The chemical shift data were also analyzed with the aim of correlating changes in chemical shifts as a function of pH and temperature with changes in the protein structure and dynamics. Chemical shift differences were calculated between data at pH 6.5 and 3.5 (at a constant temperature of 30 °C) and between data at 10 and 30 °C (at a constant pH of 6.5). For backbone ^{15}N, H^{α}, and H^{N} resonances, chemical shift differences were much larger for changes in pH (at constant temperature) than for changes in temperature (at constant pH). In changing conditions from low temperature and high pH to high temperature and low pH, the H^{α} resonances of Phe-5 and Asn-6 shift toward "statistical coil" values observed in small peptides (Wüthrich, 1986). This may result from a change in the dynamic equilibrium between three- and two-stranded β-sheets. An apparant temperature-dependent dynamic equilibrium within the structure at pH 6.5 is also monitored by changes in H^{α} chemical shifts of residues Ser-3, Phe-5, and Asn-6 between 10 and 30 °C. Overall the observed changes in chemical shifts are not easily interpreted as it appears that the resonance frequencies are very sensitive to even minor structural and dynamical differences and complicated by the effects of pH on the degree of ionization of various side chains.

At pH 6.5, there are few clearly characterized differences in the estimated values of the $^{3}J(H^{N}–H^{\alpha})$ coupling constants obtained at 10 and 30 °C (Table IV). While minor differences were observed for residues Cys-43 and His-45, most of the backbone conformation of hTGFα which can be characterized by these HSQC-J data is relatively unperturbed over this temperature range, which is well below the thermal transition temperature of 72 ± 2 °C measured by CD spectroscopy. In particular, the HSQC-J data did not provide additional evidence for a temperature-dependent dynamic equilibrium for the first strand of the N-terminal β-sheet as it was not possible to estimate the $^{3}J(H^{N}–H^{\alpha})$ coupling constant for residue Phe-5 at pH 6.5 and 30 °C, and the change in the $^{3}J(H^{N}–H^{\alpha})$ coupling constant for residue Asn-6 (Table IV)

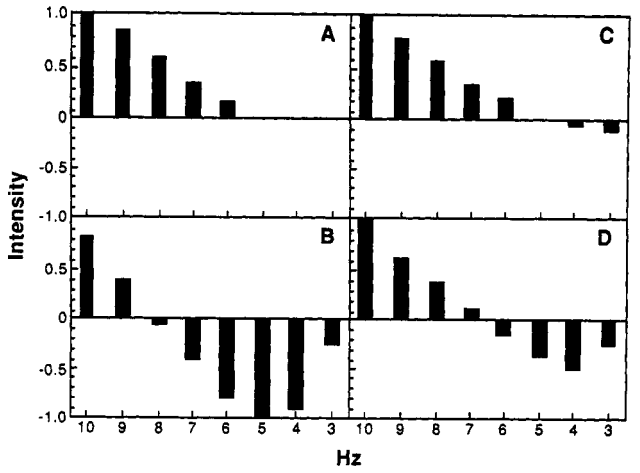

FIGURE 9: Plots of HSQC-J data for two residues exhibiting conformational differences between pH 6.5 and pH 3.5. (A) Residue Thr-13 at pH 6.5, with $^3J(H^N–H^\alpha) < 6.0$ Hz. (B) Residue Thr-13 at pH 3.5, with $^3J(H^N–H^\alpha) = 8.5 \pm 0.5$ Hz. (C) Residue Phe-15 at pH 6.5, with $^3J(H^N–H^\alpha) = 5.0 \pm 1.0$ Hz. (D) Residue Phe-15 at pH 3.5, with $^3J(H^N–H^\alpha) = 6.5 \pm 0.5$ Hz. All of these data were obtained at a temperature of 30 °C.

was smaller than the uncertainty in the estimated values at 10 and 30 °C.

The HSQC-J experiments do provide evidence for some differences between the $^3J(H^N–H^\alpha)$ coupling constants at 30 °C and pH 6.5 compared to pH 3.5. Representative data from arrays of these experiments revealing structural differences in the backbone conformations of residues Thr-13 and Phe-15 at pH 6.5 and 3.5 are presented in Figure 9. For residue Thr-13, the estimated value of the $^3J(H^N–H^\alpha)$ coupling constant shifts from <6 Hz at pH 6.5 to 8.5 ± 0.5 Hz at pH 3.5 (Figure 9). Residue Phe-15, which is in the same region of the molecule, exhibits a shift in the $^3J(H^N–H^\alpha)$ coupling constant from 5 ± 1 Hz at pH 6.5 to 6.5 ± 0.5 Hz at pH 3.5 (Figure 9). The $^3J(H^N–H^\alpha)$ coupling constant of residue Val-33, which acts as a conformational hinge residue between the N-terminal and C-terminal subdomains of hTGFα, also reflects the change in pH, shifting from 9.5 ± 0.5 Hz at pH 6.5 to <9 Hz at acidic pH. In addition, the $^3J(H^N–H^\alpha)$ coupling constant of residue Asp-47 shifts from 6.5 ± 0.5 Hz at pH 6.5 to 7.5 ± 0.5 Hz at pH 3.5.

While measurements of coupling constants could be used to characterize a few structural changes between pH 6.5 and 3.5, most $^3J(H^N–H^\alpha)$ coupling constants in hTGFα do not change significantly with pH. For residues Asp-7, Cys-8, Phe-17, Thr-20, Leu-24, Gln-26, Asp-28, His-35, Tyr-38, His-45, Ala-46, Leu-48, Leu-49, and Ala-50, the estimated values of $^3J(H^N–H^\alpha)$ coupling constants at 30 °C agree within 1 Hz at pH 6.5 and 3.5. These data are consistent with the thermal transition measurements obtained from CD spectroscopy, which indicate that the overall unfolding transition of hTGFα at pH 3.5 and 6.5 does not occur until temperatures greater than 30 °C (Figure S2). *Accordingly, the alterations in $^3J(H^N–H^\alpha)$ coupling constants between pH 3.5* and *6.5 observed for residues Thr-13, Phe-15, Val-33, and Asp-47 represent local partial unfolding of hTGFα at pH 3.5.*

Backbone–backbone NOEs, $^3J(H^N–H^\alpha)$ coupling constants, and postulated hydrogen bonds that were characterized by hydrogen/deuterium exchange measurements (Montelione et al., 1989) at pH 6.5 and 3.5 are summarized in Figure 10. Overall, these combined data indicate localized structural changes between pH 6.5 and 3.5, with general preservation of the key structural elements in hTGFα. In particular, the data reveal little or no disruption of the N-terminal antiparallel

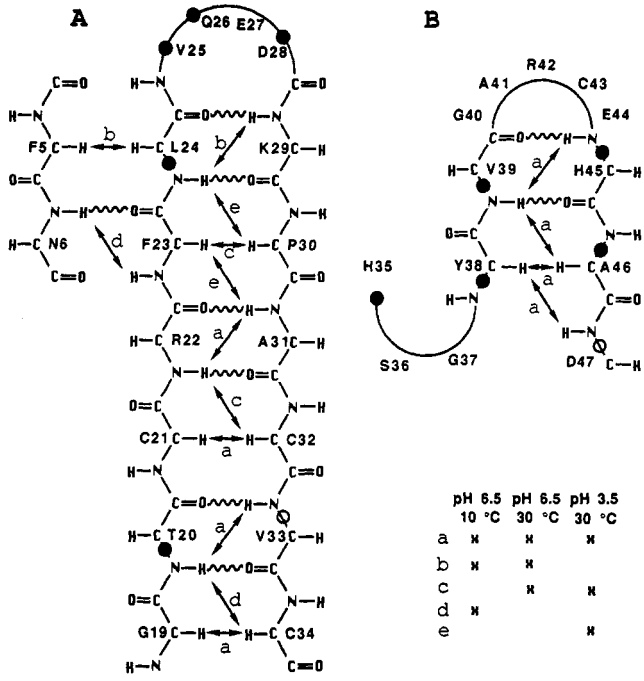

FIGURE 10: Summary of long-range backbone–backbone NOE and HSQC-J data for hTGFα at pH 6.5 and 3.5. Shown are planar schematic representations of the regular hydrogen-bonded structures in hTGFα. (A) The N-terminal triple-stranded antiparallel β-sheet. (B) The C-terminal double hairpin structure. Both of these structures are labeled with interstand hydrogen bonds (wavy lines) identified on the basis of hydrogen/deuterium exchange and NOE data. Long-range backbone–backbone NOEs are designated by double-headed arrows. The labels a–e are used to identify NOEs observed under the three different conditions studied, as summarized in the inset. A portion of the HSQC-J data obtained at a temperature of 30 °C is also summarized in the figure. Solid circles label residues for which the measured values of $^3J(H^N–H^\alpha)$ agree to within 1 Hz at pH 6.5 and 3.5. An open circle indicates that differences are observed in $^3J(H^N–H^\alpha)$ coupling constants measured at pH 3.5 and 6.5.

β-sheet involving the polypeptide segment Cys-21–Cys-32 between pH 6.5 and 3.5 (at 30 °C) and between 10 and 30 °C (at pH 6.5). The NOEs connecting the first strand of this β-sheet, polypeptide segment Phe-5–Asn-6, are not observed at pH 3.5 (30 °C). At pH 6.5 they are weaker at 30 °C than at 10 °C, which is consistent with a temperature-dependent dynamic equilibrium for the binding of this first strand to the rest of the β-sheet. In addition, the measurements of $^3J(H^N–H^\alpha)$ coupling constants described above indicate changes in dynamic structure of the polypeptide loop segment Thr-13–Phe-15 as the pH changes from 6.5 to 3.5. However, over the range of conditions studied the double hairpin structure in the C-terminal third of hTGFα (Figure 10B) is mostly unperturbed.

DISCUSSION

Description of the Solution Structure of hTGFα. The structure of hTGFα at pH 6.5 and 10 °C is characterized by two overlapping subdomains: the N-terminal subdomain (residues Val-1–His-35) containing the A (Cys-8–Cys-21) and B (Cys-16–Cys-32) disulfide loops and the C-terminal subdomain (residues Cys-34–Ala-50) containing the C (Cys-34–Cys-43) disulfide loop. The N-terminal subdomain consists of a triple-stranded antiparallel β-sheet involving interactions between polypeptide segments Phe-5–Asn-6 (strand 1) and Phe-23–Leu-24 (within strand 2) and between polypeptide segments Gly-19–Leu-24 (strand 2) and Lys-29–Cys-34 (strand 3). The central core of this β-sheet (strands 2 and 3) is an antiparallel β-hairpin structure. For the 15

ECEPP structures with negative ECEPP/3 energies, the average ϕ, ψ values in the polypeptide segment Val-25–Asp-28 are $\phi_{25} = -77°$, $\psi_{25} = -30°$; $\phi_{26} = -63°$, $\psi_{26} = -32°$; $\phi_{27} = -122°$, $\psi_{27} = 11°$; and $\phi_{28} = 37°$, $\psi_{28} = 62°$, corresponding to a type-I β-bend at Gln-26–Glu-27. This bend is somewhat distorted by the presence of a positive ϕ value for residue Asp-28. There is also a chain reversal in polypeptide segment His-18–Gly-19 which does not correspond to a standard β-bend type. The polypeptide segment Asp-7–Cys-16, which is not as well-defined as the β-sheet structure, adopts an irregular helical conformation characterized by several NOEs involving residues i to $i + 2$ and i to $i + 3$. This irregular helical conformation, which we refer to as the "loop", is attached to the triple-stranded β-sheet by the Cys-8–Cys-21 and Cys-16–Cys-32 disulfide bonds. The β-hairpin structure of the core β-sheet (strands 2 and 3) positions residues Cys-21 and Cys-32 nearby one another in space and forms a well-defined scaffold onto which the polypeptide loop segment Asp-7–Cys-16 is connected and packed. This loop contains several residues which are essential for recognition of the EGF receptor by hTGFα (DeFeo-Jones et al., 1988, 1989; Engler et al., 1990).

The C-terminal subdomain of hTGFα consists of a small antiparallel double hairpin structure (Montelione et al., 1987, 1989, 1992) involving interactions between polypeptide segments Cys-34–His-35 (strand 4), Tyr-38–Val-39 (strand 5), and His-45–Ala-46 (strand 6). Residues Ser-36–Gly-37 form a type-II β-turn with average ϕ, ψ values in the 15 ECEPP structures of $\phi_{36} = -28°$, $\psi_{36} = 138°$ and $\phi_{37} = 89°$, $\psi_{37} = 28°$. As we have suggested previously (Montelione et al., 1992), the requirement for a backbone conformation with a positive value of ϕ at position 2 in a type-II β-bend may explain why Gly-37 is strongly conserved in nearly all EGF-like protein sequences. The polypeptide segment Gly-40–Glu-44 forms a unique multiple-bend structure which has the appearance of a single turn of a left-handed helix. This unusual structure, with positive ϕ values for one or more of residues Gly-40, Ala-41, Arg-42, and Cys-43 (Table VIII), is stabilized by the Cys-34–Cys-43 disulfide bond. Residues which are important for EGF receptor recognition by hTGFα are also located in this polypeptide segment (DeFeo-Jones et al., 1988, 1989; Engler et al., 1990). A similar backbone conformation occurs in this part of the mEGF structure (Montelione et al., 1987, 1992).

The relative orientation of the N- and C-terminal subdomains is determined primarily by 32 long-range distance constraints derived from one or more NOEs between each of the following residue pairs: Phe-15 and Arg-42, Cys-16 and Arg-42, Phe-17 and Arg-42, Phe-17 and Cys-43, Phe-17 and Glu-44, His-18 and His-35, His-18 and Tyr-38, His-18 and Cys-43, Gly-19 and Cys-34, Gly-19 and His-35, and Gly-19 and Cys-43. Since many of these NOEs are between side-chain protons, the relative orientations of the backbones of the two subdomains can vary by up to ±30° with coordinated changes in the conformations of the intervening dihedral angles. This uncertainty is evident from the fact that the RMSDs for the backbone of polypeptide segments Phe-15–Cys-34 and Val-33–Asp-47 are significantly lower than for the polypeptide segment Phe-15–Asp-47, as noted in the Results section. While this uncertainty in the NMR data does not necessarily indicate motion between the subdomains, it is interesting to observe that many of the residues at the interface between polypeptide segments Phe-15–Gly-19 and Tyr-38–Glu-44 have proton resonances with broader line widths than those observed in other parts of the protein structure. Similar observations have been made for murine EGF (Montelione et al., 1987, 1992). Broadening of these resonances could be caused by interconversion between multiple side-chain conformations of the inter-subdomain interface at a rate which is intermediate on the NMR time scale. The N-terminal polypeptide segment Val-1–His-4 and the C-terminal segment Leu-48–Ala-50 are poorly defined by the available NMR data. The proton resonances in these parts of the molecule are relatively narrow and appear to be conformationally flexible. More detailed studies of nuclear relaxation will be required to substantiate these preliminary interpretations of the proton resonance line widths in these different regions of the hTGFα molecule.

Comparison with Previously Published hTGFα Structures. The chain fold of the present structure of hTGFα is similar to the hTGFα structures described by Kline et al. (1990) (15 structures of [des-Val-Val]hTGFα at pH 6.3 and a temperature of 20 °C) and by Harvey et al. (1991) (5 structures of complete hTGFα at pH 6.5 and a temperature of 30 °C). These two sets of structures were determined from 380 (81 long-range) and 383 (120 long-range) NOE-based constraints, respectively, while the structures described here are based on 357 (169 long-range) NOE-based constraints; fewer intraresidue NOEs were used in our structure determination because most of the associated constraints were too loose to provide a significant restriction of conformational space. While both of these earlier studies included stereospecific assignments for several methylene protons and isopropyl methyl groups, neither included experimental constraints on the backbone dihedral angle ϕ from $^3J(H^N–H^\alpha)$ measurements, which are obtained in our work using samples of ^{15}N-enriched hTGFα. Both sets of previously described hTGFα coordinates have been refined using restrained molecular dynamics, while we have used restrained energy minimization.

Many details of the structures of hTGFα described by Kline et al. (1990) and Harvey et al. (1991) are identical in our hTGFα structures. At the time this paper was written, coordinates for four of the structures of Kline et al. (1990) were available from the Brookhaven Protein Data Bank, while those of Harvey et al. (1991) were submitted but not yet available for distribution. All three sets of structures identify the same global chain fold, with a three-stranded antiparallel β-sheet in the N-terminal subdomain and a double hairpin structure in the C-terminal subdomain. The three groups also have identified similar chain reversals at Phe-17–Thr-20 (nonstandard), Gln-26–Glu-27 (type I), Ser-36–Gly-37 (type II), and Gly-40–His-45 (multiple bend structure which looks like one turn of a left-handed helix). As in our ECEPP structures, residues Asp-28, Gly-37, and Cys-43 have positive ϕ values in the energy-refined structures reported by Harvey et al. (1991). Our structures have been calculated from a more complete set of long-range NOE and scalar coupling constant [including 17 $^3J(H^N–H^\alpha)$ measurements] constraints and have used a larger number of starting conformations in order to ensure good sampling of the conformational space consistent with the experimental constraints. The pairwise RMSDs among our ECEPP structures are similar (for defined regions of the protein structure) to those reported in these earlier studies. For optimal superpositions of the four best Kline structures, the mean pairwise RMSDs for backbone atoms of polypeptide segments Phe-15–Asp-47, Phe-15–Cys-34, and Val-33–Asp-47 are 1.4, 1.0, and 0.7 Å, respectively. For comparison, the mean pairwise RMSDs for backbone atoms of our four best ECEPP structures for the same polypeptide segments are 1.1, 0.7, and 1.0 Å, respectively.

The backbone chain folds of our 15 ECEPP structures and the four hTGFα structures of Kline et al. (1990) are generally

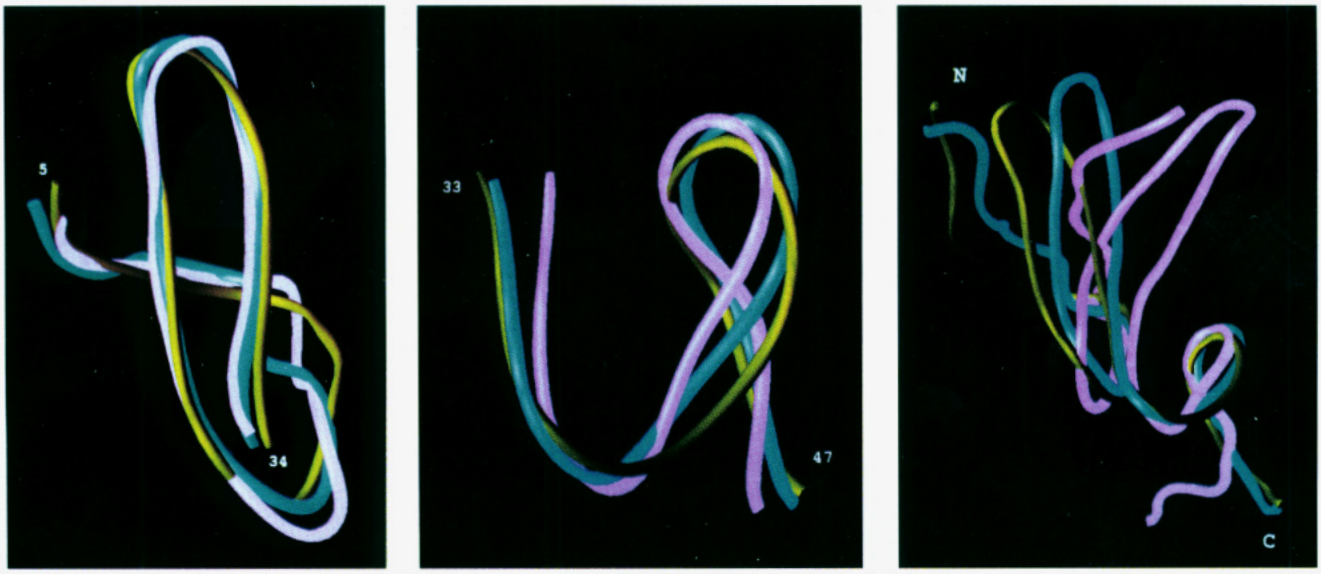

FIGURE 11: Molecular cartoons generated with the program RIBBONS (Carson, 1991) showing superpositions of the averaged backbone coordinates of hTGFα (described in this paper) in green, the averaged backbone coordinates of hTGFα determined by Kline et al. (1990) in blue, and the averaged backbone coordinates of mEGF determined by Montelione et al. (1992) in pink. (A, left) Superpositions of the averaged backbone coordinates for polypeptide segment Phe-15–Cys-34 of the hTGFα structures with polypeptide segments Tyr-13–Asn-16 and Gly-18–Cys-33 of mEGF. (B, middle) Superpositions of the averaged backbone coordinates for polypeptide segment Val-33–Asp-47 of the hTGFα structures with polypeptide segment Asn-32–Asp-46 of mEGF. (C, right) Superpositions of the averaged backbone coordinates for polypeptide segments Phe-5–Asp-47 of hTGFα and Tyr-3–Asp-46 of mEGF, generated by optimally superimposing polypeptide segment Val-33–Asp-47 of the hTGFα structures with polypeptide segment Asn-32–Asp-46 of mEGF. This last set of superimposed structures shows the differences in the relative orientations of the N-terminal subdomains when the C-terminal subdomains are optimally aligned.

similar, but there are some differences in details. The chain folds of the individual subdomains were compared by optimally superimposing within each set the backbone atoms of polypeptide segment Phe-15–Cys-34 or Val-33–Asp-47. For each of these four sets of coordinates, average coordinates were then calculated. The RMSDs between the averaged ECEPP and the averaged coordinates of Kline et al. were 1.2 and 0.9 Å for the backbone of polypeptide segments Phe-15–Cys-34 and Val-33–Asp-47, respectively. Next, the backbone atoms of the entire polypeptide segment Phe-15–Asp-47 were optimally superimposed within each of the two sets, and for each set, average coordinates were calculated. The RMSDs between the averaged ECEPP structures and the averaged structures of Kline et al. were 1.3 Å for the backbone atoms of residues Phe-15–Asp-47. *Hence the differences between the backbone structures in these independently determined NMR structures are comparable to the uncertainties in the individual structure determinations.* Figure 11 shows molecular cartoons comparing these averaged hTGFα structures.

Comparison of the Solution Structures of hTGFα at pH 6.5 and 3.5. Comparisons of the NMR parameters for hTGFα at 30 °C between pH 6.5 and 3.5 indicate partial unfolding of the protein at pH 3.5. While the major hydrogen-bonded β-sheet structures involving polypeptide segments Cys-21–Cys-32 (an antiparallel β-sheet) and His-35–Asp-47 (a double hairpin structure) are not disrupted at low pH, the polypeptide segment Val-1–Cys-8 is disordered under acidic conditions. By using ^{15}N-enriched hTGFα, we have been able to characterize small changes in backbone dihedral angles as a function of pH, providing more data on this conformational transition than have been available from previous studies (Tappin et al., 1989). These $^3J(H^N–H^\alpha)$ measurements indicate minor conformational changes in the polypeptide loop segment Thr-13–Phe-15 and in the backbone dihedral angles ϕ of residues Val-33 and Asp-47. Overall, the major backbone structural elements of hTGFα are not disrupted by changing the pH from 6.5 to 3.5 at 30 °C, even though there is shift in the dynamic conformational equilibrium of the first strand of the β-sheet involving residues Phe-5–Asn-6. These NMR studies reveal an ensemble-averaged structure of hTGFα at pH 3.5 with a backbone conformation similar to that at pH 6.5 but with a looser, more dynamic structure.

In order to provide a graphic view of the structural changes in hTGFα which occur at acidic pH, we also calculated solution structures using the DISMAN computer program as described in the Methods and Materials section. Five structures at pH 3.5 were generated from 374 conformational constraints. As there are an insufficient number of NOEs between the "subdomains" at pH 3.5 to define their relative orientations, no attempt was made to interpret the overall structure at acidic pH. The average RMSDs for backbone atoms of the N-terminal (residues Phe-15–Cys-34) and C-terminal (residues Val-33–Asp-47) subdomains at pH 3.5 are 1.8 and 1.7 Å, respectively. The backbone motifs of these hTGFα subdomains at pH 6.5 and 3.5 are compared in Figure 12. Overall, these subdomains have similar structures.

The $^3J(H^N–H^\alpha)$ coupling constant measurements indicate that the pH-induced changes in the backbone conformation of the polypeptide loop segment residues Pro-9–His-18 occur together with a change in the backbone conformation of residue Val-33. In the three-dimensional structure of hTGFα at pH 6.5, residues Phe-15–Gly-19 pack against residues Cys-34–His-35 and Arg-42–Glu-44 to form an interface between the N-terminal triple-stranded and C-terminal double hairpin subdomains of hTGFα. This interface forms a cleft which contains many residues essential for EGF-receptor recognition (Defeo-Jones et al., 1988, 1989; Engler et al., 1990). The shift from pH 6.5 to 3.5 results in structural alterations in this interface, as evidenced by $^3J(H^N–H^\alpha)$ coupling constants within the polypeptide loop segment Pro-9–His-18, located between the two subdomain structures. This reorientation may involve flexing of the polypeptide backbone of residue Val-33, which acts as a "hinge" between the two subdomains.

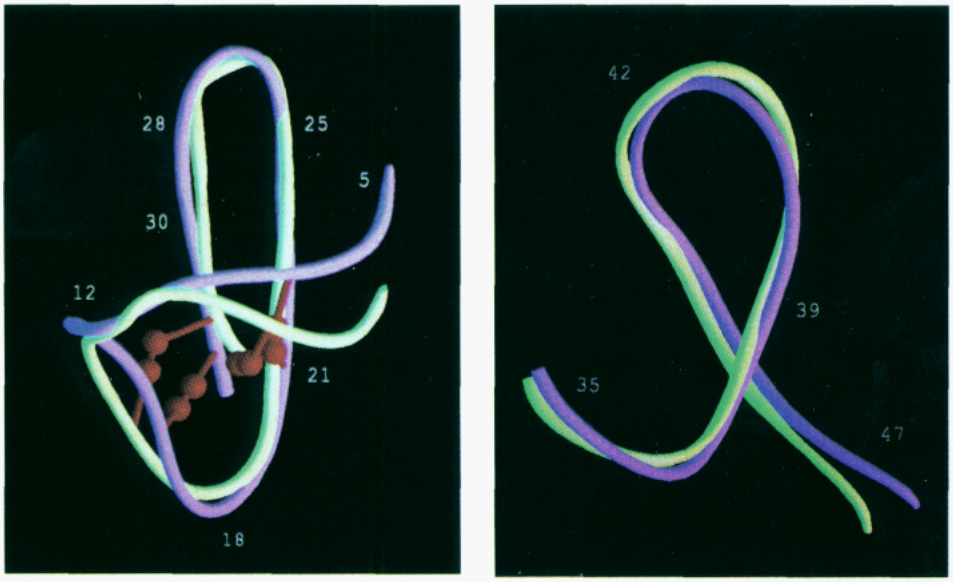

FIGURE 12: Superposition of the averaged backbone structure of hTGFα at pH 6.5 (violet) and pH 3.5 (green). (A, left) Superpositions of the averaged backbone (N, C^{α}, C′) coordinates for polypeptide segment Phe-5–Val-33. The superposition was calculated to best fit the average coordinates of polypeptide segment Cys-8–Val-33. Approximate residue locations are marked on the structures. (B, right) Superpositions of the averaged backbone (N, C^{α}, C′) coordinates for polypeptide segment His-35–Leu-48. The superposition was calculated to best fit the average coordinates of polypeptide segment His-35–Leu-48. Approximate residue locations in hTGFα are marked on the structures.

Corroborative evidence for alterations in the relative orientation and dynamics of these subdomains comes from analysis of NOESY spectra as there are many more NOEs at the interface between polypeptide segments Phe-15–Gly-19, Cys-34–His-35, and Arg-42–Glu-44 at pH 6.5 than at pH 3.5. The apparent high degree of flexibility about this hinge in hTGFα precludes use of simple distance geometry calculations to characterize reliably its overall structure at pH 3.5.

Tappin et al. (1989) have also observed that there are structural differences between hTGFα at pH 6.5 and 3.8, although their data are less extensive than those presented here and their conclusions about structural changes are therefore more limited. The major difference between pH 6.5 and 3.8 reported in their work is the disruption of the first strand of the N-terminal β-sheet at acidic pH, which is confirmed in our study of hTGFα. Tyr-38 was also observed to have a different temperature dependence of chemical shift at acidic and neutral conditions and to have a slowly exchanging amide proton at acidic pH, suggesting that at low pH values the protein interconverts between multiple conformations while maintaining a β-bend backbone structure in the polypeptide segment His-35–Tyr-38 (Tappin et al., 1989). Their 1D-NMR data also provide evidence for other changes in the dynamic structure of hTGFα which are indicated by pH-dependent changes in proton resonance line widths of many amide and H^{α} resonances. Overall, the results of this earlier study (Tappin et al., 1989) are in good agreement with our more detailed analysis of pH-induced conformational changes as characterized by many NOE and $^3J(H^N–H^{\alpha})$ coupling constant measurements. However, our data provide a more precise characterization of the locations and amplitudes of the pH-induced conformational changes in hTGFα.

Histidine–Histidine Interactions in hTGFα. Between pH 6.5 and 3.5 several side-chain functional groups change their degree of ionization. For fully solvent-accessible side chains, and in the absence of neighboring electrostatic effects, the normal pK_a's of imidazole and carboxyl groups are about 6.5 and 4.0, respectively. Hence, the changes observed in the dynamic structure of hTGFα over this pH range are probably due to titration of one or more of the five histidines, three aspartic acids, and two glutamic acid side chains. In addition, at acidic pH the molecule has many positive charges, associated with histidine, arginine, and lysine side chains, which can interact to destabilize side-chain packing interactions between the subdomains. From an examination of the three-dimensional structure of hTGFα, likely sites of pH-dependent interactions between the subdomains include residues His-18, His-35, Arg-42, Glu-44, and His-45. For these three histidine residues, pK_a values have been determined previously from 1D-NMR data (Tappin et al., 1989). The pK_a's of His-18, His-35, and His-45 are 7.6, 5.4, and 6.3, respectively. The abnormally high pK_a of His-18 has been attributed to ionic interactions with Glu-44 (Tappin et al., 1989). However, there are also several potential hydrogen bond acceptors within 3.5 Å of His-18 in some of the 16 structures of hTGFα, including the imidazole nitrogens of His-35, the phenolic oxygen of Tyr-38, and backbone carbonyl oxygens of residues Cys-43, Glu-44, and His-45. The abnormally low pK_a of His-35 can also be explained by hydrogen-bonded interactions in which one of its imidazole nitrogens acts as a hydrogen bond acceptor (Laskowski & Scheraga, 1954). Possible hydrogen bond donors that are within 3.5 Å of the His-35 imidazole nitrogens in the 16 structures of hTGFα include the side-chain imino protons of His-18 and the backbone amide protons of residues Gly-19 and Thr-20. These potential hydrogen-bonded and electrostatic interactions can account for alterations observed in the pK_a's of His-18 and His-35. In particular, the close proximity of the imidazole rings of these two residues and characteristic interplay of their pK_a values suggest that homologous hydrogen bonds (Laskowski & Scheraga, 1954) between these two histidines may play a key role in the pH-dependent interactions of the subdomains of hTGFα. In mEGF, His-18 and His-35 are replaced by Asn-16 and Val-34, respectively, and the 3D structure is relatively unchanged over the pH range from 2 to 8 (Kohda et al., 1991).

Effects of Structure and Dynamics on Chemical Shift Dispersion. Comparing the amide proton and nitrogen-15 chemical shifts of hTGFα at pH 6.5 and 3.5 reveals significant changes that are not easily correlated with the minor structural changes in the backbone conformation indicated by NOE and

scalar coupling constant measurements. This can be seen clearly by comparing the ^{15}N–^{1}H correlation spectra at pH 6.5 and 3.5 (Figure 2). This result can be rationalized by the fact that the low-pH form of hTGFα is much more flexible and that the observed chemical shifts at pH 3.5 are ensemble-averaged between ordered and multiple "disordered" conformations. The ^{15}N and ^{1}H chemical shifts appear to be much more sensitive to pH-induced changes in structure and dynamics than either NOE or $^{3}J(H^{N}–H^{\alpha})$ measurements. Additional evidence for a dynamic hTGFα structure at acidic pH is the observation that all of the amide protons, including those in interstrand hydrogen bonds, exchange relatively rapidly (i.e., with half-lives <1 h at a temperature of 30 °C) in $^{2}H_2O$ with solvent deuterons at pH 3.5 (Montelione et al., 1989). At acidic pH, the titration of the several histidine and carboxyl groups acts to destabilize side-chain packing interactions, resulting in a looser protein structure.

Cooperativity of the pH-Induced Unfolding of hTGFα. Most NMR studies of protein unfolding suggest a highly cooperative process involving a transition from fully folded to fully disordered conformational states (Montelione & Scheraga, 1989). On the other hand, the pH-induced unfolding of hTGFα is not highly cooperative and involves partially unfolded species. This is not too surprising since, under conditions of low pH and high salt, several other proteins have been observed to form dynamic structures in which the regular backbone structure is preserved while long-range packing interactions are disrupted (von Hipple & Schleich, 1969; Ahmad & Bigelow, 1979; Baum et al., 1989). Although some studies have suggested that such partially unfolded forms of proteins may correspond to intermediates in protein folding mechanisms, the role of the structures present in hTGFα at low pH in its folding mechanism cannot be evaluated from the available data.

Application of HSQC-J in Characterizing Conformational Changes in Proteins. Measurements of scalar coupling constants provide information that is complementary to NOE data in characterizing protein structures by NMR. In this work, we have used $^{3}J(H^{N}–H^{\alpha})$ coupling constants determined by HSQC-J spectroscopy to study pH-induced structural changes that are not easily characterized by NOE measurements. These represent to our knowledge the first example of using scalar coupling constant measurements to characterize partially unfolded conformations of a protein.

Comparison of the Structures of hTGFα and mEGF. We also compared the backbone chain fold of hTGFα at pH 6.5 with that of mEGF determined at pH 3.1 (Montelione et al., 1992). The mEGF sequence was aligned with hTGFα by comparing polypeptide segments Asn-1–Tyr-3, Cys-6–Asn-16, and Gly-18–Trp-49 of mEGF with polypeptide segments His-4–Asn-6, Cys-8–His-18, and Gly-19–Ala-50 of hTGFα, accounting for the deletion of mEGF residue Gly-17 in the homologous hTGFα sequence. This alignment also accounts for the fact that the first strand of the β-sheet in the N-terminal subdomain of mEGF is shifted in register by one residue compared to the homologous strand in hTGFα. Residue Pro-4 in mEGF cannot donate an interstrand hydrogen bond homologous to that of Asn-6 in the hTGFα structure, but the first strand still forms in mEGF with Tyr-3 donating the homologous hydrogen bond (Montelione et al, 1986, 1987, 1992).

A comparison of the distribution of NOE-derived inter-residue constraints in hTGFα and mEGF is presented in Figure 13. Aside from the shift in the alignment of the first strand of the β-sheet, the overall structures of hTGFα and mEGF

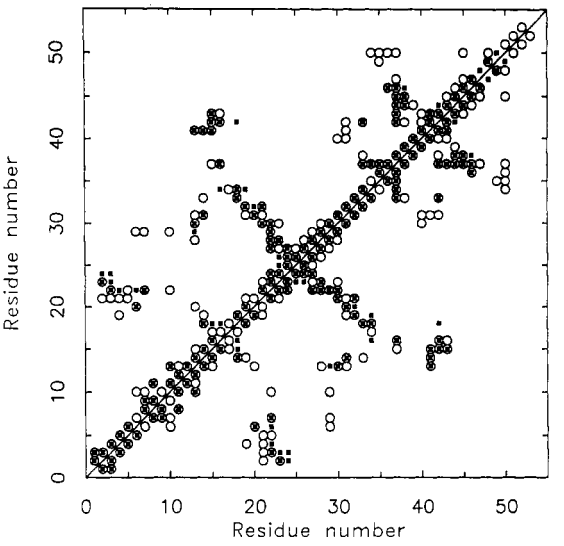

FIGURE 13: Comparison of the NOE-derived distance constraints for mEGF (Montelione et al., 1992) and hTGFα in a diagonal plot. Each axis is labeled with the amino acid sequence numbers of mEGF, and the open circles and closed squares connect pairs of residues linked by one or more cross peaks in NOESY spectra of mEGF and hTGFα, respectively.

are quite similar. Nearly all of the NOEs identified in hTGFα correspond to NOEs identified in the homologous mEGF spectra. However, many more constraints were identified for mEGF (at pH 3.1 and 28 °C), including 203 sequential and 348 long-range NOE-derived distance constraints (Montelione et al., 1992).

Averaged coordinates of the 16 energy-refined structures of mEGF were computed and compared with the average coordinates of our hTGFα structures. The β-bend types in mEGF at positions Asn-16–Gly-17 (nonstandard), Ser-25–Leu-26 (type I), and Ile-35–Gly-36 (type II) and in the polypeptide segment Gly-39–Gln-43 (multiple bend with the appearance of one turn of a left-handed helix) match the bend conformations of the corresponding segments in hTGFα. For polypeptide segment Phe-15–Cys-34 (or Val-33–Asp-47), the RMSD between the averaged hTGFα backbone atoms and the corresponding backbone atoms of mEGF was 1.7 Å (or 1.5 Å). Hence, the chain folds of the hTGFα subdomains are quite similar to those of mEGF. On the other hand, for residues Phe-15–Asp-47 the RMSD between backbone atoms of the average hTGFα structure and the corresponding backbone atoms of average mEGF structure is 3.0 Å. The large differences between backbone conformations of residues Phe-15–Asp-47 and the smaller differences for backbones of the N- and C-terminal subdomains demonstrate that there is a small but significant difference in relative orientations of the two subdomains between the mEGF and hTGFα structures. A graphic presentation of this comparison between the backbone structures of mEGF and hTGFα is shown in Figure 11.

Several key residues responsible for receptor recognition by hTGFα, including residues Phe-15 and Arg-42 (DeFeo-Jones et al., 1988, 1989; Engler et al., 1990), are at the hinge region of the interdomain cleft, and their relative positions are similar in these structures of hTGFα and mEGF. From a comparison of the NOE-derived distance constraints for these two molecules (Figure 13), we observed that the relative positions of residues 13–16 with respect to residues 41–43 (mEGF numbering) are constrained by inter-subdomain NOEs to be similar for these homologous residues of mEGF and hTGFα. Although there are significant differences in

the overall structures of hTGFα and mEGF (Figure 11C), some of the residues important for receptor recognition are brought together in space by interactions between the loop (Asp-7–Cys-16) and left-handed helical (Gly-40–Glu-44) polypeptide segments which have similar positions with respect to one another in these three structures. Perhaps the similarities and differences (Figures 11 and 13) between the structures of these growth factors account for the observation that the relative affinities of mEGF and hTGFα vary with different EGF-receptor types (Heldin & Westermark, 1990).

Several key NOEs between residues Thr-30 and Asp-40, Cys-31 and Asp-40, Cys-31 and Arg-41, and Cys-31 and Cys-42 observed for mEGF were not identified in the hTGFα NOESY spectra (Figure 13). These NOEs account for the observed differences in the relative orientations of the subdomains in the calculated structures of these homologous growth factors. However, it is not yet clear if the absence of these NOEs in NOESY spectra of hTGFα is due to real differences in the solution structures, differences in interdomain motion, or to incompleteness in the experimental data for hTGFα. Hopefully, a better understanding of these effects will result from detailed studies of internal motion based on nuclear relaxation time measurements which are now in progress.

ACKNOWLEDGMENT

We thank Dr. K. Gibson for advice and assistance in carrying out the restrained energy minimization calculations, Dr. Norma Greenfield for assistance in collecting CD data, Dr. B. Lyons for assistance in analyzing the heteronuclear NMR experiments, and Mr. G. Elkins for assistance in generating molecular graphics. We also thank Dr. S. D. Emerson, Dr. R. Williams, Ms. C. Biamonti, and Ms. J. Bumby for helpful comments on the manuscript.

SUPPLEMENTARY MATERIAL AVAILABLE

Three tables giving ^{1}H and ^{15}N chemical shift data for hTGFα and four figures showing ^{15}N-edited NMR experiments, thermal transition curves, an HSQC-TOCSY spectrum, and a comparison of H^{α} chemical shifts for hTGFα (9 pages). Ordering information is given on any current masthead page.

REFERENCES

Ahmad, F., & Bigelow, C. C. (1979) *J. Mol. Biol. 131*, 607.

Anzano, M. A., Roberts, A. B., Smith, J. M., Sporn, M. B., & De Larco, J. E. (1983) *Proc. Natl. Acad. Sci. U.S.A. 80*, 6264–6268.

Baron, M., Norman, D. G., Harvey, T. S., Handford, P. A., Mayhew, M., Tse, A. G. D., Brownlee, G. G., & Campbell, I. D. (1992) *Protein Sci. 1*, 81–90.

Baum, J., Dobson, C. M., Evans, P. A., & Hanley, C. (1989) *Biochemistry 28*, 7–13.

Billeter, M., Braun, W., & Wüthrich, K. (1982) *J. Mol. Biol. 155*, 321–346.

Billeter, M., Neri, D., Otting, G., Qian, Y. Q., & Wüthrich, K. (1992) *J. Biomol. NMR 2*, 257–274.

Bodenhausen, G., & Ruben, D. J. (1980) *Chem. Phys. Lett. 69*, 185–199.

Braun, W. (1987) *Q. Rev. Biophys. 19*, 115–157.

Braun, W., & Gō, N. (1985) *J. Mol. Biol. 186*, 611–626.

Braunschweiler, L., & Ernst, R. R. (1983) *J. Magn. Reson. 53*, 521–528.

Brown, S. C., Mueller, L., & Jeffs, P. W. (1989) *Biochemistry 28*, 593–599.

Burgess, A. W. (1989) *Br. Med. Bull. 45*, 401–424.

Campbell, I. D., Cooke, R. M., Baron, M., Harvey, T. S., & Tappin, M. J. (1989) *Prog. Growth Factor Res. 1*, 13–22.

Carson, M. (1991) *J. Appl. Crystallogr. 24*, 958–961.

Carver, J. A., Cooke, R. M., Esposito, G., Campbell, I. D., Gregory, H., & Sheard, B. (1986) *FEBS Lett. 205*, 77–81.

Cooke, R. M., Wilkinson, A. J., Baron, M., Pastore, A., Tappin, M. J., Campbell, I. D., Gregory, H., & Sheard, B. (1987) *Nature (London) 327*, 339–341.

Davis, D. G., & Bax, A. (1985) *J. Am. Chem. Soc. 107*, 2820–2821.

Defeo-Jones, D., Tai, J. Y., Wegrzyn, R. J., Vuocolo, G. A., Baker, A. E., Payne, L. S., Garsky, V. M., Oliff, A., & Rieman, M. W. (1988) *Mol. Cell. Biol. 8*, 2999–3007.

Defeo-Jones, D., Tai, J. Y., Vuocolo, G. A., Wegrzyn, R. J., Shofield, T. L., Rieman, M. W., & Oliff, A. (1989) *Mol. Cell. Biol. 9*, 4083–4086.

De Larco, J., & Todaro, G. J. (1978) *Proc. Natl. Acad. Sci. U.S.A. 75*, 4001–4005.

Derynck, R., Roberts, A. B., Winkler, M. E., Chen, E. Y., & Goeddel, D. V. (1984) *Cell 38*, 287–297.

Dubs, A., Wagner, G., & Wüthrich, K. (1979) *Biochim. Biophys. Acta 577*, 177–194.

Eich, G., Bodenhausen, G., & Ernst, R. R. (1982) *J. Am. Chem. Soc. 104*, 3731–3732.

Engler, D. A., Montelione, G. T., & Niyogi, S. K. (1990) *FEBS Lett. 271*, 47–50.

Fesik, S. W., & Zuiderweg, E. R. P. (1988) *J. Magn. Reson. 78*, 588–593.

Guntert, P., & Wüthrich, K. (1991) *J. Biomol. NMR 1*, 447–456.

Harvey, T. S., Wilkinson, A. J., Tappin, M. J., Cooke, R. M., & Campbell, I. D. (1991) *Eur. J. Biochem. 198*, 555–562.

Heldin, C. H., & Westermark, B. (1990) in *Growth Factors, Differentiation Factors, and Cytokines* (Habenicht, A., Ed.) pp 267–278, Springer-Verlag, Berlin.

Huang, L. H., Cheng, H., Pardi, A., Tam, J. P., & Sweeney, W. V. (1991) *Biochemistry 30*, 7402–7409.

Jeener, J., Meier, B. H., Bachmann, P., & Ernst, R. R. (1979) *J. Chem. Phys. 71*, 4546–4553.

Kabsch, W. (1978) *Acta Crystallogr., Sect. A 34*, 827–828.

Kay, L. E., Marion, D., & Bax, A. (1989) *J. Magn. Reson. 84*, 72–84.

Kline, T. P., Brown, F. K., Brown, S. C., Jeffs, P. W., Kopple, K. D., & Mueller, L. (1990) *Biochemistry 29*, 7805–7813.

Kohda, D., & Inagaki, F. (1988) *J. Biochem. (Tokyo) 103*, 554–571.

Kohda, D., & Inagaki, F. (1992a) *Biochemistry 31*, 11928–11939.

Kohda, D., & Inagaki, F. (1992b) *Biochemistry 31*, 677–685.

Kohda, D., Gō, N., Hayashi, K., & Inagaki, F. (1988) *J. Biochem. (Tokyo) 103*, 741–743.

Kohda, D., Shimada, I., Miyake, T., Fuwa, T., & Inagaki, F. (1989) *Biochemistry 28*, 953–958.

Kohda, D., Sawada, T., & Inagaki, F. (1991) *Biochemistry 30*, 4896–4900.

Kumar, A., Ernst, R. R., & Wüthrich, K. (1980) *Biochem. Biophys. Res. Commun. 95*, 1–6.

Laskowski, M., Jr., & Scheraga, H. A. (1954) *J. Am. Chem. Soc. 76*, 6305–6319.

Macura, S., Huang, Y., Suter, D., & Ernst, R. R. (1981) *J. Magn. Reson. 43*, 259–281.

Marion, D., Kay, L. E., Sparks, S. W., Torchia, D. A., & Bax, A. (1989) *J. Am. Chem. Soc. 111*, 1515–1517.

Mayo, K. H., Cavalli, R. C., Peters, A. R., Boelens, R., & Kaptein, R. (1989) *Biochem. J. 257*, 197–205.

Momany, F. A., McGuire, R. F., Burgess, A. W., & Scheraga, H. A. (1975) *J. Phys. Chem. 79*, 2361–2381.

Montelione, G. T., & Scheraga, H. A. (1989) *Acc. Chem. Res. 22*, 70–76.

Montelione, G. T., Wüthrich, K., Nice, E. C., Burgess, A. W., & Scheraga, H. A. (1986) *Proc. Natl. Acad. Sci. U.S.A. 83*, 8594–8598.

Montelione, G. T., Wüthrich, K., & Scheraga, H. A. (1988) *Biochemistry 27*, 2235–2243.
Montelione, G. T., Winkler, M. E., Burton, L. E., Rinderknecht, E., Sporn, M. B., & Wagner, G. (1989) *Proc. Natl. Acad. Sci. U.S.A. 86*, 1519–1523.
Montelione, G. T., Wüthrich, K., Burgess, A. W., Nice, E. C., Wagner, G., Gibson, K. D., & Scheraga, H. A. (1992) *Biochemistry 31*, 236–249.
Moy, F. J., Scheraga, H. A., Patt, S. L., & Montelione, G. T. (1992) *J. Magn. Reson. 98*, 451–457.
Müller, L. (1987) *J. Magn. Reson. 72*, 191–196.
Némethy, G., Pottle, M. S., & Scheraga, H. A. (1983) *J. Phys. Chem. 87*, 1883–1887.
Némethy, G., Gibson, K. D., Palmer, K. A., Yoon, C. N., Paterlini, G., Zagari, A., Rumsey, S., & Scheraga, H. A. (1992) *J. Phys. Chem. 96*, 6472–6484.
Neri, D., Otting, G., & Wüthrich, K. (1990) *J. Am. Chem. Soc. 112*, 3663–3665.
Piantini, U., Sørensen, O. W., & Ernst, R. R. (1982) *J. Am. Chem. Soc. 104*, 6800–6801.
Ramachandran, G. N., & Sasisekharan, V. (1968) *Adv. Protein Chem. 23*, 283–437.
Roberts, A. B., Anzano, M. A., Lamb, L. C., Smith, J. M., & Sporn, M. B. (1981) *Proc. Natl. Acad. Sci. U.S.A. 78*, 5339–5343.
Roterman, I. K., Lambert, M. H., Gibson, K. D., & Scheraga, H. A. (1989) *J. Biomol. Struct. Dyn. 7*, 421–453.
Scheraga, H. A. (1992) *Int. J. Quantum Chem. 42*, 1529–1539.
Selander, M., Persson, E., Stenflo, J., & Drakenberg, T. (1990) *Biochemistry 29*, 8111–8118.
Simpson, R. J., Smith, J. A., Moritz, R. L., O'Hare, M. J., Rudland, P. S., Morrison, J. R., Lloyd, C. J., Grego, B., Burgess, A. W., & Nice, E. C. (1985) *Eur. J. Biochem. 153*, 629–637.
Sporn, M. B., & Todaro, G. J. (1980) *N. Engl. J. Med. 303*, 878–880.
Sporn, M. B., & Roberts, A. B. (1985) *Nature (London) 313*, 745–747.
Tappin, M. J., Cooke, R. M., Fitton, J. E., & Campbell, I. D. (1989) *Eur. J. Biochem. 179*, 629–637.
von Hipple, P. H., & Schleich, T. (1969) *Biol. Macromol. 2*, 417.
Wagner, G. (1982) *J. Magn. Reson. 55*, 151–156.
Williamson, M. P., Havel, T. F., & Wüthrich, K. (1985) *J. Mol. Biol. 182*, 295–315.
Winkler, M. E., Bringman, T., & Marks, B. J. (1986) *J. Biol. Chem. 261*, 13838–13843.
Wüthrich, K. (1986) *NMR of Proteins and Nucleic Acids*, Wiley, New York.
Wüthrich, K., Billeter, M., & Braun, W. (1983) *J. Mol. Biol. 169*, 949–961.